Comparative poly(A)+ RNA interactome capture of fission yeast RNA exosome mutants reveals insights into RNA biogenesis

Adrien Birot[1], Cornelia Kilchert[2], Krzysztof Kus[1], Emily Priest[1], Ahmad Al Alwash[1], Dong-Hyuk Heo[1], Alfredo Castello[1], Shabaz Mohammed[1], and Lidia Vasiljeva[1]*.

[1] Department of Biochemistry, University of Oxford, Oxford OX1 3QU, UK
[2] Institute of Biochemistry, Justus-Liebig University Giessen, Giessen, Germany.

* To whom correspondence should be addressed. Tel: +44 1865 613352; Email: lidia.vasilieva@bioch.ox.ac.uk

ABSTRACT

The nuclear RNA exosome plays a key role in quality control and processing of multiple protein-coding and non-coding transcripts made by RNA polymerase II. A mechanistic understanding of exosome function remains a challenge given it has multiple roles in RNA regulation. Here we have analysed changes in the poly(A)+ RNA transcriptome and interactome provoked by mutations in three distinct subunits of the nuclear RNA exosome. We have identified multiple proteins whose occupancy on RNA is altered in the exosome mutants. We demonstrate that the Zinc-finger protein Mub1 regulates exosome dependent transcripts that encode stress-responsive proteins. Furthermore, we assess impact of the exosome inactivation upon RNA binding of the components of the mRNA processing machineries such as spliceosome and mRNA cleavage polyadenylation complex. We show that mutations in the exosome lead to accumulation of the components of U1 and U2 snRNPs on poly(A)+ RNA and depletion of the components of the activated spliceosome from RNA suggesting that the early stages of spliceosome assembly might provide a critical quality control step. Collectively, our data provide a global view of how RNA metabolism is affected in the exosome-deficient cells and reveal RNA-binding proteins that may act as novel exosome cofactors.

INTRODUCTION

Regulation of RNA maturation and degradation is crucial to accurate gene expression (1). The nucleolytic RNA exosome complex has a central role in monitoring nearly multiple types of transcripts produced by RNA polymerase I, II, and III (Pol I, II, and III) (2–9). The nuclear RNA exosome functions in RNA processing (3'end trimming) of stable non-coding (nc) RNA species such as ribosomal RNAs (rRNAs), transfer RNAs (tRNAs), telomerase RNA, small nuclear and nucleolar RNAs (snRNAs and snoRNAs) and quality control where it degrades precursors of unprocessed or incorrectly processed mRNA and ncRNAs produced by all three polymerases (2–11). The Exosome also degrades the unstable products of cryptic transcription (Cryptic Unstable Transcripts, CUTs) (12–15). Recent studies have also demonstrated that the exosome not only removes unprocessed mRNAs but is also required for proper mRNA processing since exosome mutants show splicing and mRNA 3'end processing defects (16–20). Finally, it has also been recently demonstrated that the exosome regulates the levels of specific mRNA transcripts in response to environmental changes and is an important player in executing specific gene expression programmes during development (9, 20–24). Unsurprisingly, mutations in the nuclear exosome lead to severe neurological diseases in humans, such as spinal muscular atrophy and pontocerebellar hypoplasia (24, 25).

The nuclear RNA exosome is a 3′–5′ exonuclease complex that consists of a 9-protein catalytically inactive core complex (EXO-9) and two catalytic subunits, Rrp6 (EXOSC10), and Dis3/Rrp44 (hDIS3). EXO-9 forms a double-layered barrel-like structure that comprises six ribonuclease (RNase) (PH)-like proteins (Rrp41, Rrp42, Rrp43, Rrp45, Rrp46, and Mtr3) and three S1/K homology (KH) "cap" proteins (Rrp4, Rrp40, and Csl4) (26). The two catalytic subunits occupy opposite ends of EXO-9 to constitute EXO-11 (27, 28). Rrp6 is located at the top of the S1/KH cap ring near the RNA entry into the channel formed by the exosome cap and core, and Dis3 is found at the bottom of EXO-9 channel near the RNA exit pore. Both Rrp6 and Dis3 are 3′–5′ exonucleases, but the latter also has endonucleolytic activity (2). In yeast, Rrp6 is restricted to the nucleus and Dis3 is found in both nuclear and cytoplasmic compartment (29, 30).

The conserved helicase Mtr4 is essential for RNA degradation by the exosome, however, the mechanism underpinning Mtr4 function in exosome regulation is not well understood (31). In the fission yeast, *Schizosaccharomyces pombe* (*S. pombe*), Mtr4 shares its function with the highly homologous Mtr4-like helicase (Mtl1) (32). Mtr4/Mtl1 interacts with the RNA-binding proteins and the exosome and was proposed to play a role in exosome recruitment to substrate RNAs (1). The exosome-bound Mtr4 facilitates the unwinding of the RNAs substrates and their threading through the channel (33, 34). In addition to the exosome core, Mtr4/Mtl1 co-purifies with the RNA binding proteins involved in substrate recognition. In *Saccharomyces cerevisiae* (*S. cerevisiae*), Mtr4 is a part of the TRAMP complex (Trf4/5–Air1/2–Mtr4) which consists of two Zinc-finger proteins Air1 and Air2 (only Air1 in fission yeast), poly(A) polymerases Trf4 and Trf5 and Mtr4 (35–37). The TRAMP complex is recruited to RNA by the RNA and Pol II-binding protein Nrd1 during transcription (15, 38–41). However, in contrast to *S. cerevisia*e, the TRAMP complex seems more specialized in regulation of

rRNA processing in fission yeast and human (31). In fission yeast, Mtl1 is proposed to interact with the Zinc-finger protein Red1 to constitute the Mtl1-Red1 complex (MTREC) (32, 42).

Additionally, Mtl1 interacts with the conserved YTH-domain containing protein Mmi1 and associated proteins, Red1, Iss10 and Erh1 (12, 32, 42–44). Mmi1 is needed for degradation of a selected group of mRNAs encoding for proteins involved in meiosis, cell cycle regulation, biosynthetic enzymes, RNA biology and ncRNAs by the exosome. Mmi1 is co-transcriptionally recruited to these transcripts by binding to an UUAAAC sequence motifs known as 'determinants of selective removal' (DSRs), and this is proposed to lead to their degradation (20, 21, 23, 45). Mmi1 is also important for mRNA quality control and in particular for degradation of inefficiently spliced mRNAs and proper transcription termination of selected transcripts (16, 20, 46). In addition to Mmi1, Iss10, Erh1 and Red1, Mtl1 also co-purifies with other factors that have been functionally linked to the exosome regulation: the Zinc-finger protein Red5, the poly(A) binding protein Pab2, RRM (RNA-Recognition-Motif) and PWI (Pro-Trp-Ile signature) domain containing protein Rmn1 and the CAP-binding proteins Cbc1, Cbc2 and Ars2 (12, 32). Although complexes these proteins form have not been well defined biochemically, Mtl1 has been proposed to be a part of several distinct modules including Mtl1-Red1-Pab2-Red5-Rmn1, Mtl1-Red1, Mtl1-Red1-Mmi1-Iss10-Erh1 and Mtl1-Red1-Cbc1-Cbc2-Ars2. Nevertheless, the mechanisms by which these factors regulate substrate recognition and exosome targeting to substrate RNAs remain obscure. In addition to a group of RNAs regulated by Mmi1, levels of multiple other transcripts have been reported to increase in nuclear exosome mutants suggesting that additional Mmi1-independent mechanisms could contribute to their recognition (12, 32). Here, we demonstrate that a subpopulation of these depends on the zing-finger-MYND (myeloid, Nervy, and DEAF-1) domain protein Mub1 for decay.

To gain further insight into function and regulation of the nuclear RNA exosome, we have compared the poly(A)+ transcriptomes and poly(A)+ RNA-bound proteomes from control and three different exosome mutants (*mtl1-1*, *rrp6Δ* and *dis3-54*). Our analyses support a functional connection between Rrp6 and Mtl1 in controlling levels of multiple mRNAs and ncRNAs as well as H/ACA snoRNA maturation in addition to regulation of unstable ncRNAs (CUTs) previously suggested for nuclear exosome (12). Our data suggest that nuclear exosome plays more prominent role in controlling fission yeast transcriptome than previously anticipated. Interestingly, analyses of the changes in poly(A)+ bound proteome induced by the exosome mutants have identified potential novel factors related to exosome regulation in fission yeast. We focus on the uncharacterised zf-MYND protein Mub1, which is highly enriched on poly(A)+ RNA in the exosome mutant. Mub1 physically interacts with the exosome and its deletion leads to up-regulation of a specific subset of exosome substrates supporting its role in exosome regulation. Furthermore, we have analysed the data to assess whether occupancy of the RNA binding components of RNA processing machineries is affected in the exosome mutants. We report that the components of the NineTeen Complex (NTC) involved in activation of the spliceosome for catalysis are depleted from RNAs in contract to components of U1 and U2 snRNPs suggesting that the stage prior to the activation of the spliceosome is affected in the exosome mutants and might represents a critical quality control step during splicing. Finally, we also assess RNA-

binding behaviour of factors linked to exosome function. We show that RNA recognition can be uncoupled from subsequent steps involved in exosome targeting to RNAs upon inactivation of Mtl1 by mutations in *mtl1-1*. While engagement with the RNA is lost for the exosome and Mtl1 in this mutant, factors proposed to be involved in substrate recognition (Mmi1, Iss10) as well as some other RNA-binding exosome factors such as Cbc1, Cbc2, Ars2 and Red1 remain on RNA. These data argue for a two-step mechanism leading to the exosome recruitment to its substrates. Altogether, our data provide insights into different aspects of RNA regulation by the exosome as well as furthers our understanding of the mechanism underpinning exosome function.

RESULTS

Poly(A)+ RNA interactome capture in the exosome mutants.

To gain further insights into how the exosome contributes to RNA regulation, we have applied an unbiased quantitative proteomic approach, called RNA interactome capture (RIC), and identified proteins directly interacting with polyadenylated RNA (poly(A)+) in WT cells and in three exosome mutants: *rrp6Δ*, lacking exonuclease Rrp6; *dis3-54*, a Dis3 mutant which contains an amino acid substitution (Pro509 to Leu509) located within RNB domain that was reported to show reduced catalytic activity (47, 48) and *mtl1-1,* a mutant of the helicase Mtl1, which has mutations in the region surrounding the arch domain (32) (Figure 1A). The underlying hypothesis behind this approach was that inactivation of the exosome would not only stabilise RNAs targeted by the exosome but also affect RNA occupancy of the proteins that are functionally linked to the exosome (Figure 1B). The three mutant strains were cultured alongside a WT control in the presence of 4-thiouracil (4sU) to facilitate RNA-protein crosslinking with 365nm UV light. Following UV crosslinking, poly(A)+ RNA was enriched by oligo-d(T) selection and RNA-associated proteins were identified by mass spectrometry (Figure 1B). The abundance of individual proteins in the whole cell extract (WCE) was also determined by proteomics and used to normalise the RIC data (see Material and Methods) as in (49, 50). The RIC/WCE ratio was used to determine the enrichment profile reflected the association of each individual protein with RNA in the mutants relative to the WT (Supplementary Table 1). Additionally, RNA sequencing was carried out for oligo-d(T) enriched samples to assess levels of polyadenylated RNAs in mutant and WT cells (Figure 1B).

As proof of principle, we assessed if crosslinking of the RNA-binding protein Mmi1, a known exosome regulatory RNA-binding factor involved in substrate recognition, that was found to be enriched in the WT poly(A)+ RNA interactome (49), has been affected in the exosome mutant. This analysis has demonstrated further 1.5, 2 and 4 times increase of Mmi1 association with poly(A)+ RNA (*p*-value=0.768, *p*-value=0.039 and *p*-value=0.001) in the exosome mutants *dis3-54*, *mtl1-1* and *rrp6Δ* RIC respectively, compared to WT cells (Figure 1C). The increased poly(A)+ RNA association of Mmi1 in exosome mutants correlates with the increased abundance of Mmi1 RNA substrates as revealed by the analysis of oligo-d(T)-enriched RNAs from these strains by deep sequencing (RNA-

seq) (Figure 1D). Indeed, Mmi1 mRNAs targets were most noticeably enriched in the *rrp6Δ* and *mtl1-1* mutants compared to the *dis-54* mutant. These results demonstrate that changed RNA occupancy of individual proteins identified through comparative poly(A)+ RNA interactome analysis can potentially be used for the identification of RNA-bound factors related to the exosome.

To further assess how mutations in different exosome subunits affect levels of poly(A)+ RNA globally, we analysed poly(A)+ RNA-seq data more closely. Consistent with the function of the exosome in degradation of ncRNAs (snRNAs, snoRNAs, antisense RNA), levels of these transcripts were increased in all three exosome mutants (Figure 2A, Supplementary Table 3). Interestingly, a high number of mRNAs is also increased in the exosome mutants more than 1.5-fold suggesting that the nuclear exosome regulates multiple mRNAs in addition to its known role in degradation of ncRNAs (Figure 2B, Supplementary Figure S1A-B) (12, 32). Compared to *rrp6Δ* and *mtl1-1* mutants, less RNAs are increased in *dis3-54* mutant, possibly reflecting an only partial loss of Dis3 function in this mutant under conditions tested. Furthermore, the large fraction of the transcripts increased in *rrp6Δ* was also increased in *mtl1-1* (corresponding to ~80% of RNAs increased in Mtl1 mutant) in agreement with the suggested functional connection between Mtl1 and Rrp6 (32) . Interestingly, approximately half of the transcripts increased in Dis3 mutant (54%) is also dependent on Mtl1. Although this corresponds to a smaller fraction of Mtl1 regulated transcripts (25%) this is likely due to milder effect of P509L mutation on Dis3 function in *dis3-54* mutant. Our data supports a model where Mtl1 regulates both exosomes associated nucleases, with Rrp6 being perhaps slightly more dependent on Mtl1 compared to Dis3.

We next performed comparative analysis of proteins differentially enriched in all three interactomes. For each RIC triplicate, proteins that are detected at least in two out of three biological repeats of this experiment are used in the analysis leading to a total number of 1146 proteins considered (see Material and Methods). From this analysis, 206, 247 and 138 were enriched more than 2-fold in *mtl1-1*, *rrp6Δ* and *dis3-54* compared to WT respectively (Supplementary Table 2). On the other hand, we detected 196, 147 and 137 proteins whose abundance on poly(A)+ RNA was reduced in *mtl1-1*, *rrp6Δ* and *dis3-54* (Supplementary Table 2). Consistently with the RNA-seq data, higher overlap was observed between proteins whose RNA binding is affected in *rrp6Δ* and *mtl1-1* than between *dis3-54* and *mtl1-1*. These results further support a functional link between Mtl1 and Rrp6 (Figure 2C-D).

Next, we performed gene ontology (GO) analyses across the three different mutants to assess whether proteins with altered RNA-binding in the exosome mutants are part of a specific biological process. The analysis has revealed that nuclear proteins are most noticeably affected in all three exosomes mutants including *dis3-54* mutant where both nuclear and cytoplasmic forms of the exosome are compromised (Figure 2E, Supplementary Table 4). This suggests that the exosome plays a prominent role in nuclear RNA metabolism. Consistently, Mtl1 and Rrp6 exosome mutants show accumulation of poly(A)+ RNA inside the nucleus, which is in agreement with previously published observations (Figure 2F and Supplementary Figure S1C-D) (51–53). In contrast, *dis3-54* shows modest poly(A)+ RNA accumulation in the nucleus (Figure 2E and Supplementary Figure

S1D). This might indicate that Dis3 plays less dominant role in regulation of RNA in the nucleus compared to Mtl1 and Rrp6. However, milder nuclear retention of poly(A)+ RNA observed in *dis3-54* compared to other exosome mutants might be due to only partial inactivation of Dis3 in this mutant as discussed above. Interestingly, even though only mild accumulation of poly(A)+ RNA is observed, increased RNA-binding of nuclear proteins is more pronounced compared to cytoplasmic proteins in *dis3-54* (Figure 2E). This might reflect that exosome has more prominent impact on nuclear rather than cytoplasmic RNPs. Additionally, RNA-binding activity of proteins related to mRNA metabolic process (GO:0016071), ribosome biogenesis (GO:0042254) and cytoplasmic translation (GO:0002181) is altered in all mutants (Supplementary Table 4).

Altogether, this analysis reveals that proteins affected in each specific mutant tend to be linked to similar biological processes. Additionally, these data demonstrate significant changes in RNA-protein interactions in exosome deficient cells, highlighting the important role of the exosome in RNA metabolism.

Comparative RIC reveals novel proteins that are linked to the exosome.

We hypothesised that comparative RIC approach can be employed to identify novel RNA-bound exosome factors by assessing protein enrichment on poly(A)+ RNA in the exosome mutants. We first selected proteins that were more than 2-fold enriched on poly(A)+ RNA in the interactome of at least one mutant. Second, we focussed on proteins containing a classical RNA-binding domains (54) and annotated as uncharacterised. This resulted in a list of 10 potentials candidates (Figure 3A).

Next, the candidate genes were deleted to test whether they recapitulate phenotypes associated with compromised exosome function. We have assessed steady-state levels of RNAs that are up-regulated in the exosome mutants but are independent of known exosome factor Mmi1 (such as the RNA produced from the Tf2 retro-transposable element (*SPAC9.04*)). Increase in *tf2-1* RNA levels is observed in *SPBC31F10.10c*Δ and *SPBC16G5.16*Δ compared to WT (Figure 3B, compare lanes 7 and 11 to lane 1). *SPBC31F10.10c* encodes for Mub1 protein, which contains an Armadillo-type domain, and a potential nucleic acid binding region represented by a zf-MYND domain. Mub1 shows a >6-fold increase in *mtl1-1* RIC (*p*-value= 5,41E-08) (Figure 3A) suggesting that it might be linked to Mtl1 function.

Next, we have assessed whether nuclear retention of poly(A)+ RNA, a typical phenotype of the exosome mutants, can be recapitulated in the deletion strains using poly(A)+ FISH (Figure 3C). Deletion of six candidates, namely *srp40*, *SPCC126.11c*, *pof8*, *SPBC530.08*, *SPBC16G5.16*, and *swt1*, resulted in moderate nuclear retention of poly(A)+ RNA compared to WT and *rrp6*Δ (Figure 3C and Supplementary Figure S2A).

Exosome mutants have been demonstrated to show defects in heterochromatic silencing (32, 55). This results in accumulation of heterogeneous RNAs produced from telomeric and centromeric regions of the *S. pombe* genome, although the underlying mechanism remains unclear. To test whether the candidate proteins might contribute to expression of heterochromatic transcripts, each

individual deletion mutant was crossed with the strain bearing a *ura4+* reporter gene inserted within transcriptionally silent telomeric region of chromosome I. We then monitored the capacity of these reporter strains to grow on -URA plates or plates containing 5-Fluoroorotic acid (5-FOA) at 25°C and 30°C. Interestingly, the deletion of either *SPAC126.11c*, *srp40* or *SPAC222.18* led to moderate growth on –URA plates and attenuated growth on 5-FOA compared to WT (Figure 3D and Supplementary Figure S2B), suggesting that each of these candidates might play a role in heterochromatin formation/maintenance. It is interesting to note that *SPAC126.11c* and *srp40* deletion cells also showed nuclear retention of poly(A)+ RNA (Figure 3C). Both SPAC126.11c and Srp40 were also previously reported to co-purify with the exosome further supporting a direct link between these proteins and the exosome (42, 56).

Taken together, this preliminary screen has identified several candidate proteins, including SPBC31F10.10c, SPAC126.11c, Srp40 or SPAC222.18, whose deletions phenocopy exosome mutants suggesting a potential relationship between these factors and the nuclear RNA exosome. However, further studies are needed to test whether this is indeed the case.

Mub1 regulates exosome degradation of the stress-induced mRNAs.

To further understand how Mub1 contributes to RNA regulation we have investigated the functional consequences of Mub1 deletion. Interestingly, *mub1* deleted cells showed a rounded morphology, suggesting an alteration in processes related to cell morphology (Supplementary Figure S3A). To assess the contribution of Mub1 in regulation of RNA levels we carried out transcriptome analyses by RNA-seq in WT and *mub1Δ*, *mtl1-1* and double mutant (*mtl1-1 mub1Δ*). RNA-seq data was normalised to *S. cerevisiae* spike-in for calibration (see Material and Methods). This analysis has revealed that 248 transcripts (162 mRNAs and 86 ncRNAs) are upregulated more than 1.5-fold (p-value<0.05) in *mub1Δ* cells (Figure 4A, Supplementary Tables 5-6). Interestingly, many transcripts that are affected by Mub1 deletion were also increased in *mtl1-1* (Figure 4A-B) suggesting that Mtl1 and Mub1 act in the same pathway. In agreement with RNA-seq data, increased steady-state levels of *gst2* and *SPCC663.08c* mRNAs in *mub1Δ* and *mtl1-1* mutants is also detected by northern blot analyses (Figure 4B). No additive effect was observed in the double mutant *mtl1-1 mub1Δ* compared to single mutants, which is consistent with Mtl1 and Mub1 acting together (Figure 4B). To assess whether Mub1 and the exosome directly interact, we carried out co-immunoprecipitation experiments. These experiments have revealed that Mub1 co-purifies with the Rrp6 subunit of the exosome supporting a physical link between Mub1 and the nuclear exosome (Figure 4C).

Presence of Mub1 in the poly(A)+ RNA interactome suggests that Mub1 is an RNA-binding protein. Mub1 contains a predicted zf-MYND domain (471-528), which is likely to mediate its interaction with RNA. We therefore hypothesised that this domain may be critical for Mub1 function. To test this, we deleted the zf-MYND domain of Mub1 (Figure 4D). Deletion of the zf-MYND domain led to expected change in size of the protein, which was assessed by visualising FLAG tagged protein by Western blotting (Figure 4E). Addition of triple FLAG tag to Mub1 didn't have any effect on cell morphology, cell growth and cellular protein levels (Supplementary Figure S3A-C).The protein level of

Mub1Δ471-528-3xFLAG (Mub1-ΔZ-3xFLAG) was comparable to Mub1-3xFLAG, suggesting that the deletion did not affect the stability of the truncated protein (Figure 4E). Cells expressing the truncated Mub1Δ471-528-3xFLAG displayed the characteristic rounded shape, alike *mub1Δ* cells suggesting that function of Mub1 is compromised in this mutant (data not shown). To test the importance of the zinc-finger domain for Mub1 function, we assessed levels of *gst2* and *SPCC663.08c* mRNAs in *mub1Δ471-528-3xFLAG* mutants by northern blot. This experiment revealed that similar to *mub1Δ,* levels of both mRNAs were increased in the *mub1Δ471-528-3xFLAG* mutant (Figure 4F). Taken together, these results suggest that Zinc-finger domain of Mub1 is essential for Mub1 function.

Mub1 plays a role in the heat shock response.

GO analysis of mRNAs increased in *mub1Δ* cells have shown a significant enrichment for GO "Core Environmental Stress Response induced" (46.25% (74/160), *p*-value = 1.55246e-28, AnGeLi tool (57)) implying that Mub1 may be required for cellular response to stress. Consistently, *mub1Δ* growth at 37°C is impaired (Figure 5A). To further assess a role of Mub1 in the regulation of genes related to heat shock, we analysed expression of *hsp16*, encoding a heat shock protein implicated in cellular response to heat (58). Indeed, *hsp16* levels are increased in *mub1Δ* and *mtl1-1* (Figure 5B, compare lanes 2-4 to 1). Interestingly, *hsp16* mRNA levels are also altered during heat shock (4 hours at 37°C) in the *mub1Δ* and *mtl1-1* (compare lanes 6-7 to lane 5), suggesting that Mub1 is required for exosome dependent expression of the heat shock genes. Interestingly, similar to complete Mub1 ablation, deletion of the zf-MYND domain also impaired growth at 37°C (Figure 5C) suggesting that this domain is required to ensure proper expression of stress response genes at 37°C.

Processing of H/ACA box snoRNA depends on Rrp6 and Mtl1.

Next, we wanted to assess how RNA binding of the known RNA-binding proteins implicated in the RNA metabolism is affected in the exosome mutants. One of the function of the nuclear RNA exosome is 3'end trimming of the precursors of the stable non-coding RNAs such as snRNAs and snoRNAs (59). Precursor molecules are polyadenylated in contrast to mature sn/snoRNAs lacking poly(A) tails (4). Indeed, increased levels of snoRNAs especially noticeable for H/ACA box snoRNAs are observed in *mtl1-1* and *rrp6Δ* compared to WT (Figure 6A). Analysis of an individual gene, *snR92*, shows that accumulation of the polyadenylated *snR92* precursor coincides with the loss of the mature form in *mtl1-1* but not in *rrp6Δ* and *dis3-54* mutants (Figure 6B and 6C, compare lanes 1 and 3). This data suggest that Mtl1 is involved in the processing of *snR92*, where it might play a role different from Rrp6 and Dis3. In contrast to *mtl1-1*, *rrp6Δ* and *dis3-54* mutants accumulate both the *snR92* precursor and the mature form of this RNA, suggesting that both Rrp6 and Dis3 control levels of mature H/ACA box snoRNAs in addition to their processing (Figure 6C, compare lanes 1-4). No accumulation of precursor or reduction in mature *snoR69b* is observed in *mtl1-1* (Figure 6C, compare lanes 5 and 6) suggesting that Mtl1 plays a less prominent role in C/D box snoRNAs processing. Interestingly, proteins that are known to bind H/ACA box snoRNAs, such as Nhp2, Nop10 and Cbf5, are strongly

enriched in the poly(A)+ interactome in *mtl1-1* and *rrp6Δ*, suggesting that these proteins are associated with pre-snoRNAs (Figure 6D-E). This is consistent with the reported co-transcriptional assembly of these proteins on H/ACA box snoRNAs and their role in snoRNA biogenesis (60). The same tendency is observed for C/D box RNA-binding proteins (Nop58, Nop56, Fib1, Pop7 and Bcd1), although the effect is less prominent compared to components of H/ACA box snoRNP (Figure 6E). These observations are in agreement with C/D box RNAs being less affected in the exosome mutants compared to H/ACA box snoRNAs and demonstrates that behaviour of protein components of RNPs reflects changes in the levels of the corresponding RNA. To assess whether compromised 3' end processing influences remodelling of H/ACA box pre-snoRNPs, we analysed RNA association of factors that are recruited at later stages of snoRNP assembly such as Gar1 protein which replaces the assembly factor Naf1. Recruitment of Gar1 to snoRNP has been proposed to complete the formation of functional H/ACA box snoRNPs (61, 62). In agreement with the observed accumulation of pre-snoRNAs, Naf1 (SPBC30D10.15 in *S. pombe*) is strongly enriched on poly(A)+ RNA in the *mtl1-1* and *rrp6Δ* interactomes. Surprisingly, we also noticed an increased association of Gar1 with poly(A)+ RNA in *mtl1-1*, where very little mature snoRNAs can be detected (Figure 6E), suggesting that Gar1 is recruited to pre-snoRNA and its recruitment is not sufficient to dissociate Naf1. In contrast, the accumulation of poly(A)+ pre-snoRNAs did not correlate with increased association of Gar1 with poly(A)+ RNA in the *rrp6Δ* interactome. This data suggest that Mtl1 may contribute to suppress the premature exchange of Naf1 and Gar1 on unprocessed transcripts. Altogether, these data highlight the important role of the nuclear exosome in H/ACA snoRNAs processing and further support functional connection between Mtl1 and Rrp6 to process this specific class of ncRNA.

Association of mRNA processing factors with poly(A)+ RNA is altered in the exosome mutants.

Previous studies have demonstrated that splicing of selected pre-mRNAs is compromised in the exosome mutants, although the direct involvement of the exosome is still under debate (18, 20). To study spliceosome recruitment to RNA in the exosome mutants, we next analysed RNA association of the splicing factors. One of the mRNAs whose splicing has been found to be compromised in *dis3-54*, *mtl1-1* and *rrp6Δ*, is *rps2202* mRNA that encodes for the 40S ribosomal protein S15a (Figure 7A-B). Spliceosome assembly is initiated upon the recognition of the intronic features such as the 5' splice site (5'ss) and the branch point (BP) by U1 and U2 snRNPs through base pairing. Recruitment of U1 and U2 to pre-mRNA is followed by association of tri-snRNP U4-U6-U5 to form the pre-catalytic B complex. One of the key steps during spliceosome assembly is the recruitment of the NineTeen Complex (NTC, or Prp19 complex, (GO:0000974)) accompanied by the dissociation of U4 and U1, which leads to the activation of the B complex for catalysis of the first trans-esterification reaction (Figure 7C) (63). Interestingly, while components of U1 and U2 snRNPs (specific proteins for U1 snRNP (GO:0005685) and U2 snRNP (GO:0005686)) are enriched, components of NTC are depleted in the *mtl1-1* interactome (Figure 7C). This data suggests that the activation of the spliceosome for catalysis is likely to be compromised upon inactivation of the exosome, potentially defining a time window for quality control.

Accumulation of longer poly(A) tails for individual RNA substrates upon mutation or depletion of the exosome subunits was reported in fission yeast and human cells (20, 64, 65). Transcripts produced by Pol II are polyadenylated by the Cleavage and Polyadenylation Factor (CPF). CPF consists of three functionally distinct activity-based modules: poly(A) polymerase, nuclease and phosphatase modules and cleavage factors CFIA and CFIB (Figure 7D) (66, 67). In addition, selected transcripts can also be polyadenylated by the non-canonical poly(A) polymerases Trf4 and Trf5 that are part of the TRAMP complex (68). However, RNA hyperadenylation observed in *rrp6Δ* is maintained in TRAMP mutants but lost when poly(A) polymerase of the CPF is compromised (12, 65). This suggest that CPF is responsible for addition of longer poly(A) tails rather than TRAMP. Consistent with the prominent role of the CPF in hyperadenylation, RNA-binding components of the CPF polyadenylation module (Iss1/Fip1, Pfs2 and Yth1) (49) are significatively enriched on poly(A)+ RNA in exosome mutants whereas TRAMP component Air1 are not (Figure 7E). Moreover, nuclease module and cleavage factors as well as an additional CPF component, Seb1 (69, 70) are also highly enriched in exosome mutants (Figure 7F). To assess whether increased association of the CPF with poly(A)+ RNA corelates with global increase in hyperadenylation we have analysed length of the poly(A) tails of cellular RNAs in Rrp6 mutant. This analysis has revealed a strong increase in the length of poly(A) tails, suggesting that global hyperadenylation of RNAs takes place in the absence of Rrp6 (Figure 7G). At the same time, polyadenylated RNA accumulates in the nucleus of the exosome mutants (Figure 2F and Supplementary Figure S1C-D). Taken together, this might indicate that in the absence of functional exosome, nuclear accumulation of RNAs prevents CPF recycling. Defect in CPF recycling could be a possible reason behind hyperadenylation of RNAs as well as defective cleavage at poly(A) site by the CPF that could subsequently lead to Pol II failure to terminate transcription as previously reported in the exosome mutants (16, 17).

Mtl1 is needed for exosome targeting and/or engagement with RNA substrates but not for RNA recognition by the RNA-binding factors.

The essential helicase Mtl1 (fission yeast) or Mtr4 (human) is important for exosome function and we show that majority of the substrates of the nuclear RNA exosome accumulate in the *mtl1-1* mutant (Figure 2B and Supplementary Figure S1A-B). Interestingly, previous studies have shown that Mtl1 can be pulled down with the exosome and also with proteins involved in RNA recognition, such as Mmi1 (12, 32). This suggests that Mtl1 could be involved in either RNA recognition or exosome targeting to RNA or both of these steps that we predict to precede degradation of the RNA by the exosome. To gain further insight into Mtl1 function, we next analysed association of factors functionally linked to the exosome with poly(A)+ RNA in the *mtl1-1* interactome (Figure 8A) (24, 38, 50). Strikingly, while the interaction of Mtl1 and the exosome subunits with poly(A)+ RNA is decreased in *mtl1-1*, association of factors involved in RNA recognition such as Mmi1, the Mmi1-associated proteins Iss10, Red1 and the CAP-binding complex Cbc1/2-Ars2 with RNA is either increased or unaffected in the absence of functional Mtl1 (Figure 8B). In addition, Mmi1, Cbc1/2-Ars2 and Red1 are also enriched on RNA in *rrp6Δ* and *dis3-54* mutants. These data suggest that exosome targeting and engagement with RNA but not RNA recognition by the RNA-binding proteins such as Mmi1 is

likely to be affected in the *mtl1-1* mutant. We therefore propose that Mtl1 plays a role in coupling RNA recognition to exosome recruitment (Figure 8C). Finally, RNA association of the exosome factors proposed to interact with poly(A) tail such as Pab2 and Red5 is decreased in exosome mutants (Figure 8D) suggesting that exosome either directly or indirectly contributes to assembly of these factors with RNA.

DISCUSSION

Controlling levels of functional RNA is a critical and essential process for all kingdoms of life. Number of RNAs produced per cell can be regulated through transcriptional and post-transcriptional mechanisms, the latter greatly relying on the multi-subunit exosome complex.

It is becoming increasingly clear from the recent research that in addition to its housekeeping function in generation of functional fully matured transcripts and removal of aberrant RNAs, exosome plays a role in facilitating cellular interactions with the environment. Recent study proposed that exosome is required for cell survival during heat shock through the proper expression of cell wall integrity (CWI) genes in budding yeast (71). Furthermore, exosome was shown to be implicated in heat sock response in flies suggesting that function of the exosome in environmental adaptation is conserved (72). In addition to heat shock, exosome has been shown to play a role in cellular responses to nutrients, cell differentiation or DNA damage response in budding yeast and human (16, 73–76). Although, these studies have revealed a prominent role of post-transcriptional regulation in mediating these responses, the underlying mechanisms responsible for selective regulation of the specific transcripts are currently not well understood. Our analysis has identified the RNA-binding protein Mub1 importance for the exosome dependent regulation of a subset of stress response genes in fission yeast, which helps to understand how these transcripts are regulated by the exosome and further highlights the important contribution of the nuclear RNA exosome in mediating adaption to environmental changes.

How does Mub1 contributes to the exosome regulation? We show that the zinc-finger domain of Mub1 is important to drive Mub1 function. Similar to Mub1, multiple factors associated with the exosome contain Zinc-finger domains. In fission yeast these are the component of the TRAMP Air1, Red1 and Red5 proteins (43, 77, 78). Zinc-finger domain of Red1 and Red5 were shown to be important for RNA degradation by the exosome as mutations in this region leads to RNA stabilisation (43, 78). Furthermore, mutations in Zinc-finger domain of *S. cerevisiae* Air1 and another Zinc-finger component of TRAMP complex Air2 leads to loss of interaction with Trf4, compromised integrity of the TRAMP complex and stabilisation of the exosome substrate RNAs *in vivo* suggesting that Zinc-finger domain might also function in mediating protein-protein interactions within exosome regulatory complexes in addition to RNA binding (79). In human cells, multiple Zinc-finger proteins have been found to play a role in exosome regulation. This includes ZCCHC7 (homologue of Air2), ZC3H18, ZCCHC8, ZC3H3 and ZFC3H1 supporting an evolutionary conserved role for these proteins in exosome regulation (80–

82). ZCCHC8 interacts with RNA binding protein RMB7 and helicase MTR4 to form the trimeric Nuclear EXosome Targeting (NEXT) (81, 83). ZFC3H1 and ZC3H3 form Poly(A) Tail eXosome Targeting (PAXT) complex with MTR4, poly(A) binding protein PABN1 and RNA binding proteins RMB26/27 (53, 82, 84, 85). In addition to the Zinc-finger domain, ZCCHC8 also contains a hydrophobic region called “arch interacting motif” (AIM) that mediates interaction with MTR4 arch domain and the C-terminal region that stimulates helicase activity of MTR4 (86, 87). AIM region is also present in other exosome co-factors- ZCCHC7 (Air2), rRNA processing factors NOP53 and NVL (88, 89). It is possible that similar to other Zinc-finger proteins involved in exosome regulation, Mub1 could help to ensure the connection between the exosome and its target RNAs by mediating contacts with RNA and other proteins involved in exosome regulation such as Mtl1. Mub1 also has another domain in addition to MYND-type Zinc-finger domain- Armadillo-like helical domain. Future studies will clarify the specific role of Mub1 and its domains in the exosome regulation. Based on our findings, we propose a model in which Mub1 acts as an exosome co-factor involved either in substrate recognition and/or exosome targeting to a subset of RNAs that are induced in response to stress.

One of the key factors that is essential for the function of the nuclear exosome is the RNA helicase Mtr4/Mtl1. Two models of how Mtr4 assist RNA degradation by the exosome have been proposed based on the recent structural studies of reconstituted human and *S. cerevisiae* exosomes: 1) MTR4 recruitment to the core of human exosome mediates substrate channelling to DIS3 and is mutually exclusive with substrate channelling to RRP6 and RRP6 association with the top of the exosome core (33), 2) Mtr4 interacts with Rrp6, as has been demonstrated for the *S. cerevisiae* exosome (34). Our data suggest that in fission yeast, Mtl1 is required for both Rrp6 and Dis3 function *in vivo*. In agreement with our findings, it has recently been shown that the expression of Rrp6-GFP-Mmi1 chimeric protein is sufficient to supress the dysregulated expression of meiotic genes in a Mtl1 mutant (*mtl1-cs5*) and *red1Δ* mutants (90). Furthermore, we demonstrate that Rrp6 and Mtl1 mutants accumulate unprocessed precursors of H/ACA box snoRNAs suggesting that both proteins cooperate to mediate 3’-end maturation of these transcripts. Notably, accumulation of pre-snoRNAs correlates with enrichment of the components of pre-snoRNPs in poly(A)+ pull-downs observed in these mutants. Indeed, Nop10, Nhp2, Cbf5 and the snoRNP assembly factor *S. pombe* Naf1 (SPBC30D10.15) were strongly enriched in both interactomes compared to WT. It has been suggested by previous studies that the protein Gar1 replaces Naf1 during the maturation process of H/ACA snoRNA (60). Interestingly, while Naf1 is enriched in both the *mtl1-1* and *rrp6Δ*, Gar1 is only enriched in *mtl1-1* interactome, suggesting that Mtl1 might mediate factor exchange during snoRNA processing.

Exosome mutants have been associated with phenotypes spanning diverse defects in RNA biogenesis including pre-mRNA splicing, 3’end processing and mRNA export from the nucleus, some of which may not be directly related to exosome function (16, 20, 69, 70). Interestingly, we observe altered association of splicing factors with RNA which might explain splicing defects previously reported in exosome mutants for selected transcripts (20). We demonstrate that the factors required for activation of the spliceosome for catalyses (NTC components) are depleted from RNAs. At the

same time, association of U1-U2 components is not affected in the exosome deficient mutants. This suggests that activation of the spliceosome for catalysis might be a rate limiting step. We propose that NTC recruitment could provide a regulatory step that contributes to the regulation of the rate of splicing and might link splicing rate and decay. Interestingly, Mtl1 was shown to interact with spliceosome components, some of which are part of the NTC complex (32, 42, 91). However, at this stage, we also cannot entirely rule out a possibility for a direct recruitment of NTC by the exosome. Another reason for failed RNA processing could be titration of the RNA-binding proteins by various RNAs that accumulate in exosome mutants. In agreement with this idea, we also show, that components of the CPF machinery, responsible for addition of the poly(A) tail to the 3'end of Pol II transcribed transcripts, are enriched on poly(A)+ RNA in the exosome mutants. This suggest that CPF recycling might be compromised in the exosome mutants and could explain why RNA hyperadenylation and 3'end extension is observed in the exosome mutants. In agreement with this idea, accumulation of nuclear RNAs upon exosome depletion was proposed to be a reason behind transcriptional de-repression of the Polycomb targets in mouse ESC (92).

Although a number of factors have been linked to the exosome, their role in exosome regulation is not well understood. We demonstrate that exosome factors proposed to be involved in RNA recognition such as Mmi1 and its associated protein Iss10, as well as components of the CAP binding complex (Cbc1/2 and Ars2), remain bound to RNA in the Mtl1 mutant, whereas association of the exosome complex and Mtl1 itself is dramatically compromised. This data suggests that although Mtl1 was found to co-IP with Mmi1, it is not involved in RNA recognition and rather it might be playing a role in exosome targeting and engagement with RNA. Mtl1 was proposed to form the MTREC complex together with Red1. Interestingly, association of Red1 with poly(A)+ RNAs is increased in the Mtl1 mutant, while Mtl1 itself is not recruited to RNA. This suggests that Red1 is recruited to RNA independently of Mtl1 and reinforces the model of a two-steps recruitment of the nuclear exosome onto its RNAs substrates (Figure 8C).

It is interesting to note that a recent study has assessed changes in the poly(A)+ RNA interactome caused by RNAi depletion of the RRP40 subunit of the exosome in human cells (85). In agreement with our observations, this study reports that loss of the exosome leads to an increased RNA association of the selected exosome regulatory factors such as MTR4, ZFC3H1 (Red1) and CBC-ARS complex. Interestingly, this study also identifies new exosome co-factors in human cells (ZC3H3, RBM26 and RBM27) that are involved in linking the exosome to the PAXT complex.

Collectively, our data suggest that an RNA interactome capture approach can provide valuable insights into how the exosome might contribute to RNA regulation. Based on our data, we propose a two-step mechanism responsible for the recognition and targeting of the RNA substrates of nuclear exosome for degradation. First, RNA substrates are recognised by the RNA-binding specificity factors and second, the exosome is recruited to RNA in Mtl1-dependent manner. We also propose a key role for the NTC in monitoring the rate of mRNA splicing. Finally, we identify Mub1 as an important protein that regulates a specific class of exosome dependent mRNAs implicated in the stress response fully supporting a key role of the nuclear exosome in cell adaptability and response to environment.

MATERIAL AND METHODS

Yeast strains and manipulations

General fission yeast protocols and media are described in (93). All strains are listed in Supplementary Table 7. Experiments were carried out using YES medium at 30°C unless stated otherwise. Gene deletions and epitope tagging were performed by homologous recombination using polymerase chain reaction (PCR) products (94). All oligos are listed in Supplementary Table 8. Protein extracts and western blotting were done as described in (95), and protein co-immunoprecipitation as described in (96).

Northern blotting

Northern blot experiments were essentially performed as described in (39). RNA was prepared as described in (20). 8 µg of RNA was resolved on a 1.2% agarose gel containing 6.7% formaldehyde in MOPS buffer. After capillary transfer in 10× SSC onto a Hybond N+ membrane (GE Healthcare), RNA was UV-crosslinked and stained with methylene blue to visualise ribosomal RNA bands. For snoRNAs analysis, 16µg of RNA was resolved in 8% Urea-PAGE. Electro-transfer was performed in TBE overnight onto a Hybond N+ membrane (GE Healthcare, RPN303B). Gene-specific probes were generated by random priming in the presence of ATP [α_{32}P] using the Prime-It II Random Primer Labeling Kit (Agilent, 300385) using PCR generated DNA template produced from gDNA isolated from a wild type *S.pombe* strain (YP71) using oligonucleotides listed in Supplementary Table 8. Probes were added to the membrane and hybridized at 42°C overnight. After repeated washes in 2× SSC, 0.1% SDS, blots were exposed with Amersham Hyperfilm MP (GE Healthcare, 28-9068-44).

Poly(A)+ RNA interactome capture

Poly(A)+ *S. pombe* RNA interactome capture (RIC) was obtained from (49, 97). Briefly, two sets of triplicate experiments (Wild-type 1 (WT1) + *mtl1-1* = First eXperiment (FX); WT2 + *rrp6Δ* + *dis3-54* = Second eXperiment (SX)) were performed. *S. pombe* cells were grown at 30°C, in Edinburgh minimal media supplemented with glutamic acid (EMMG) with limited amounts of uracil (10 mg/l), and labelled with a final concentration of 1 mg/l 4-thiouridine for 4.5 h. Cells were harvested by filtration, snap-frozen in liquid nitrogen after UV-crosslinking at 3J/cm_2 in 50 ml PBS and lysed by grinding in liquid nitrogen. Clear lysates were resuspended in oligo-d(T) lysis buffer (20 mM Tris–HCl pH 7.5, 500 mM LiCl, 0.5% Lithium Dodecyl Sulfate (LiDS), 1 mM EDTA; 5 mM DTT, protease inhibitor cocktail IV (fungal) 1:10,000; 5 mM DTT). 1/48$_{th}$ of total volume of whole cell extract (WCE) was used for proteomics analysis, the rest was subjected to pull-down with oligo-d(T)x25 magnetics beads (NEB-S1419S), 1ml of slurry per 1L of cell culture during 1 hour at 4°C. Immobilized oligo-d(T)x25 magnetics beads were washed two times with oligo-d(T) wash buffer 1 (20 mM Tris–HCl pH 7.5, 500 mM LiCl, 0.1% LiDS, 1 mM EDTA, 5 mM DTT) at 4°C, two times with oligo-d(T) wash buffer 2 (20 mM Tris–HCl pH 7.5, 500 mM LiCl, 1 mM EDTA) at room temperature and two times with oligo-d(T) low salt buffer (20 mM Tris–HCl pH 7.5, 200 mM LiCl, 1 mM EDTA) at room temperature. RNA-proteins

complexes were eluted from beads with oligo-d(T) elution buffer (20 mM Tris–HCl pH 7.5,1 mM EDTA), 330µl/L of culture during 10min at 55°C. 1/33 of the oligo-d(T) pull-down total volume was used for RNA sequencing analysis. The rest was subjected to RNase-A and RNase T1 treatment and subjected to mass spectrometry analyses as described in (49).

Statistical data analysis

Statistical analysis was performed essentially as described in (40) with the following modifications. To be considered for the analysis, protein was required to be present in at least one of the interactomes with two non-zero values. Raw intensities were log2 transformed, normalised to the same median and analysis was followed by the imputation of missing values using a minimal value approach (MinDet – where each sample is considered independently). Data manipulations, principal component analysis (PCA) and Pearson correlation plots were performed with the DEP package implemented in R (1). Median-normalised data values were used to estimate the log-fold changes between exosome mutants and WT cells, which were further normalised by the whole-cell extract values (WCE-normalisation). To minimise the batch effects control experiments (WT cells) were performed twice in triplicates alongside each of the sets of exosome mutants (First triplicate = FX = WT1 + *mtl1-1*; Second triplicate = SX = WT2 + *rrp6Δ* + *dis3-54*). To test the changes between whole-cell extract normalised (WCE-normalised) proteomes of mutants and WT cells, we used modified scripts from the DEP package. Briefly, this software takes advantage of the Limma package that calculates moderated t-statistics on a linear model fit to the expression data (98). It allows defining custom contrasts (like comparing the difference of differences – as in the case of the WCE-normalised intensities). Proteins with a log2 (WCE-normalised RIC of exosome mutant/ WCE-normalised RIC of WT) > 1 were considered specifically enriched in exosomes mutants. Remaining figures and analyses were performed with custom scripts or ones modified from the DEP package. *S. pombe* GO term annotations and information on individual proteins were retrieved using PomBase (99).

Poly(A)+ RNA Fluorescence In Situ Hybridization (FISH)

Poly(A)+ RNA FISH was done as described in (100, 101), using oligo-d(T)(x20)-alexa488 (Invitrogen 7206906) DNA probe. Briefly, 5×10–1×10^8 cells were used for one hybridization reaction. Cells from an asynchronously growing culture were fixed by the addition of paraformaldehyde into the culture to a final concentration of 4%. Cell pellet was washed with 1ml of buffer B (1.2 M sorbitol, 100 mM KH_2PO_4 at pH 7.5, 4 °C) and immediately after, cell were resuspended in 1ml of spheroplast buffer (1.2 M sorbitol, 100 mM KH_2PO_4 at pH 7.5, 20 mM vanadyl ribonuclease complex and 20 µM β-mercaptoethanol) with 1% 100T zymolyase (MP Biomedicals, 083209-CF) and cell wall was digested for 60min. The reaction was stopped by washing with 1 ml of cold buffer B. Cells were incubated for 20 min in 0.01% Triton-X100/1X PBS and washed with 10% formamide/2× SSC at room temperature. Before hybridization, 50 ng of the oligo-d(T) probe was mixed with 2µl of a 1:1 mixture between yeast transfer RNA (10 mg/ml, Life Technologies, AM7119) and salmon-sperm DNA (10 mg/ml, Life Technologies, 15632-011) and the mixture was dried in a vacuum concentrator. Hybridization buffer F

(20% formamide, 10 mM $NaHPO_4$ at pH 7.0; 50 µl per hybridization) was added, and the probe/buffer F solution was incubated for 3 min at 95 °C. Buffer H (4× SSC, 4 mg/ml BSA (acetylated) and 20 mM vanadyl ribonuclease complex; 50 µl per hybridization) was added in a 1:1 ratio to the probe/buffer F solution. Cells were resuspended in the mixture and incubated overnight at 37 °C. After three washing steps (10% formamide/2× SSC; 0.1% Triton-X100/2x SSC and 1x PBS), cells were resuspended in 1× PBS/DAPI and mounted into glass slides for imaging. *Z*-planes spaced by 0.2 µm were acquired on a Ultraview spinning-disc confocal. Acquisition was done with DAPI filter (405nm) and a FITC filter (488nm for alexa488 acquisition). Images were analysed using ImageJ software (102).

Bulky poly(A) tail length measurement

RNA was prepared as for Northern blotting experiments. Bulk RNAs were 3' end labelled essentially as described in (103). Briefly, 1µg of total RNA was incubated 18h at room temperature with 2µCi of Cytidine 3', 5' bis(phosphate)-[5'-^{32}P] (^{32}pCp), T4 RNA ligase (NEB, M0204S), 10mM ATP and T4 RNA ligase buffer (NEB, M0204S) containing 10% DMSO final. Following this incubation, the 3' end labelled RNAs were simultaneously treated with 80U of RNase T1 (Thermo Fisher EN0542) and 4 µg of RNase A (Sigma Aldrich, 10109142001) in 10mM Tris-HCl (pH 7.5), 300mM NaCl and 40µg of yeast tRNA (10 mg/ml, Life Technologies, AM7119) during 2h at 30°C, to degrade RNA except for the poly(A)-tails. Following the reaction, poly(A) RNA was purified by using RNA Clean and Concentrator (Zymo research, R1017) and run on 8% Urea-PAGE gel as described before.

RNA sequencing

For spike-in normalisation, the *S. cerevisiae* cells were added to *S. pombe* at 1:10 ratio prior to RNA isolation. Total RNA was extracted from cultures in mid-log phase using a standard hot phenol method and treated with RNase-free DNase RQ1 (Promega, M6101) to remove any DNA contamination. For total RNA sequencing, experiments were done in duplicates, and ribodepletion was performed using ribominus transcriptome isolation kit (Invitrogen, K155003). Poly(A)+ RNA sequencing was performed by using 1/33 of the oligo-d(T) pull-down total volume, subjected to proteinase K treatment for 1h at 50°C. Poly(A)+ RNA was recovered by a standard hot phenol method. Experiments were done in triplicate. cDNA libraries were prepared using NEBNext® Ultra™ II Directional RNA Library Prep Kit for Illumina (NEB#E7760S) for 50ng of total RNA and using the NEBNext Ultra Directional RNA Library Prep Kit for Illumina (NEB #E7420) for 100ng of WT1, *mtl1-1*, *rrp6Δ* and *dis3-54* purified oligo-d(T) RNA. Paired-end sequencing was carried out on the Illumina HiSeq 500 platform. RNA sequencing data are available with the GEO number GSE148799 and GSE149187.

RNA-seq data analyses

Quality trimming of sequenced reads was performed using Trimmomatic (Galaxy Version 0.32.3, RRID:SCR_011848). Reads were aligned to the concatenated *S. pombe* (ASM294v2.19) using

Bowtie 2 (TopHat) (104).For spike-in normalisation, reads derived from different *S. pombe* and *S. cerevisiae* chromosomes were separated. Reads mapped only once were obtained by SAMTools (105) and reads were mapped to the genome using genome annotation from (106). Differential expression analyses were performed using DESeq2 (107) in R and using the spike-in normalisation. For poly(A)+ RNA sequencing total read count normalisation using DEseq2 (107) in R was used. The significance of RNAs list overlaps was calculated using a standard Fisher's exact test, For gene ontology analysis, up or downregulated protein coding gene lists were submitted to AnGeLi (http://bahlerweb.cs.ucl.ac.uk/cgi-bin/GLA/GLA_input), a web based tool (57).

ACCESSION NUMBERS

Raw (fastq) and processed sequencing data (bedgraph) can be downloaded from the NCBI Gene Expression with the GEO number GSE148799 and GSE149187. Mass spectrometry data are available via ProteomeXchange with identifier PXD016741.

ACKNOWLEDGEMENT

We thank the National Bio Resource Yeast Project, S. Grewal, K. Nasmyth, P. Bernard and JP. Javerzat for strains and constructs. We thank members of the Vasilieva's laboratory and Jean-Paul Javerzat for their valuable comments on the manuscript. We acknowledge the Micron Advanced Bioimaging Unit (supported by the Wellcome Strategic Awards 091911/B/10/Z and 107457/Z/15/Z) for their support and assistance in performing FISH experiments described in this manuscript.

FUNDING

This work was supported by the Wellcome Trust Senior Research fellowships [WT106994MA to L.V.] and a Medical Research Council career development award [MR/L019434/1 to A.C.].

CONFLICT OF INTEREST

None declared

REFERENCES

1. Kilchert,C., Wittmann,S. and Vasiljeva,L. (2016) The regulation and functions of the nuclear RNA exosome complex. *Nat. Rev. Mol. Cell Biol.*, **17**, 227–239.

2. Chlebowski,A., Lubas,M., Jensen,T.H. and Dziembowski,A. (2013) RNA decay machines: the exosome. *Biochim. Biophys. Acta*, **1829**, 552–560.

3. Mitchell,P., Petfalski,E., Shevchenko,A., Mann,M. and Tollervey,D. (1997) The exosome: a conserved eukaryotic RNA processing complex containing multiple 3'-->5' exoribonucleases. *Cell*, **91**, 457–466.

4. Allmang,C., Kufel,J., Chanfreau,G., Mitchell,P., Petfalski,E. and Tollervey,D. (1999) Functions of the exosome in rRNA, snoRNA and snRNA synthesis. *EMBO J.*, **18**, 5399–5410.

5. Kiss,D.L. and Andrulis,E.D. (2010) Genome-wide analysis reveals distinct substrate specificities of Rrp6, Dis3, and core exosome subunits. *RNA*, **16**, 781–791.

6. Schneider,C., Kudla,G., Wlotzka,W., Tuck,A. and Tollervey,D. (2012) Transcriptome-wide analysis of exosome targets. *Mol. Cell*, **48**, 422–433.

7. Szczepińska,T., Kalisiak,K., Tomecki,R., Labno,A., Borowski,L.S., Kulinski,T.M., Adamska,D., Kosinska,J. and Dziembowski,A. (2015) DIS3 shapes the RNA polymerase II transcriptome in humans by degrading a variety of unwanted transcripts. *Genome Res.*, **25**, 1622–1633.

8. Isken,O. and Maquat,L.E. (2007) Quality control of eukaryotic mRNA: safeguarding cells from abnormal mRNA function. *Genes Dev.*, **21**, 1833–3856.

9. Gudipati,R.K., Xu,Z., Lebreton,A., Séraphin,B., Steinmetz,L.M., Jacquier,A. and Libri,D. (2012) Extensive degradation of RNA precursors by the exosome in wild-type cells. *Mol. Cell*, **48**, 409–421.

10. Coy,S., Volanakis,A., Shah,S. and Vasiljeva,L. (2013) The Sm Complex Is Required for the Processing of Non-Coding RNAs by the Exosome. *PLOS ONE*, **8**, e65606.

11. Tseng,C.-K., Wang,H.-F., Schroeder,M.R. and Baumann,P. (2018) The H/ACA complex disrupts triplex in hTR precursor to permit processing by RRP6 and PARN. *Nat. Commun.*, **9**.

12. Zhou,Y., Zhu,J., Schermann,G., Ohle,C., Bendrin,K., Sugioka-Sugiyama,R., Sugiyama,T. and Fischer,T. (2015) The fission yeast MTREC complex targets CUTs and unspliced pre-mRNAs to the nuclear exosome. *Nat. Commun.*, **6**, 1–11.

13. Wyers,F., Rougemaille,M., Badis,G., Rousselle,J.-C., Dufour,M.-E., Boulay,J., Régnault,B., Devaux,F., Namane,A., Séraphin,B., *et al.* (2005) Cryptic pol II transcripts are degraded by a nuclear quality control pathway involving a new poly(A) polymerase. *Cell*, **121**, 725–737.

14. Neil,H., Malabat,C., d'Aubenton-Carafa,Y., Xu,Z., Steinmetz,L.M. and Jacquier,A. (2009) Widespread bidirectional promoters are the major source of cryptic transcripts in yeast. *Nature*, **457**, 1038–1042.

15. Vasiljeva,L., Kim,M., Terzi,N., Soares,L.M. and Buratowski,S. (2008) Transcription termination and RNA degradation contribute to silencing of RNA polymerase II transcription within heterochromatin. *Mol. Cell*, **29**, 313–323.

16. Shah,S., Wittmann,S., Kilchert,C. and Vasiljeva,L. (2014) lncRNA recruits RNAi and the exosome to dynamically regulate pho1 expression in response to phosphate levels in fission yeast. *Genes Dev.*, **28**, 231–244.

17. Lemay,J.-F., Larochelle,M., Marguerat,S., Atkinson,S., Bähler,J. and Bachand,F. (2014) The RNA exosome promotes transcription termination of backtracked RNA polymerase II. *Nat. Struct. Mol. Biol.*, **21**, 919–926.

18. Nag,A. and Steitz,J.A. (2012) Tri-snRNP-associated proteins interact with subunits of the TRAMP and nuclear exosome complexes, linking RNA decay and pre-mRNA splicing. *RNA Biol.*, **9**, 334–342.

19. Castelnuovo,M., Zaugg,J.B., Guffanti,E., Maffioletti,A., Camblong,J., Xu,Z., Clauder-Münster,S., Steinmetz,L.M., Luscombe,N.M. and Stutz,F. (2014) Role of histone modifications and early termination in pervasive transcription and antisense-mediated gene silencing in yeast. *Nucleic Acids Res.*, **42**, 4348–4362.

20. Kilchert,C., Wittmann,S., Passoni,M., Shah,S., Granneman,S. and Vasiljeva,L. (2015) Regulation of mRNA Levels by Decay-Promoting Introns that Recruit the Exosome Specificity Factor Mmi1. *Cell Rep.*, **13**, 2504–2515.

21. Chen,H.-M., Futcher,B. and Leatherwood,J. (2011) The Fission Yeast RNA Binding Protein Mmi1 Regulates Meiotic Genes by Controlling Intron Specific Splicing and Polyadenylation Coupled RNA Turnover. *PLOS ONE*, **6**, e26804.

22. Yang,X., Bayat,V., DiDonato,N., Zhao,Y., Zarnegar,B., Siprashvili,Z., Lopez-Pajares,V., Sun,T., Tao,S., Li,C., *et al.* (2020) Genetic and genomic studies of pathogenic EXOSC2 mutations in the newly described disease SHRF implicate the autophagy pathway in disease pathogenesis. *Hum. Mol. Genet.*, **29**, 541–553.

23. Harigaya,Y., Tanaka,H., Yamanaka,S., Tanaka,K., Watanabe,Y., Tsutsumi,C., Chikashige,Y., Hiraoka,Y., Yamashita,A. and Yamamoto,M. (2006) Selective elimination of messenger RNA prevents an incidence of untimely meiosis. *Nature*, **442**, 45–50.

24. Boczonadi,V., Müller,J.S., Pyle,A., Munkley,J., Dor,T., Quartararo,J., Ferrero,I., Karcagi,V., Giunta,M., Polvikoski,T., *et al.* (2014) EXOSC8 mutations alter mRNA metabolism and cause hypomyelination with spinal muscular atrophy and cerebellar hypoplasia. *Nat. Commun.*, **5**.

25. Wan,J., Yourshaw,M., Mamsa,H., Rudnik-Schöneborn,S., Menezes,M.P., Hong,J.E., Leong,D.W., Senderek,J., Salman,M.S., Chitayat,D., *et al.* (2012) Mutations in the RNA exosome component gene EXOSC3 cause pontocerebellar hypoplasia and spinal motor neuron degeneration. *Nat. Genet.*, **44**, 704–708.

26. Makino,D.L., Baumgärtner,M. and Conti,E. (2013) Crystal structure of an RNA-bound 11-subunit eukaryotic exosome complex. *Nature*, **495**, 70–75.

27. Januszyk,K. and Lima,C.D. (2014) The eukaryotic RNA exosome. *Curr. Opin. Struct. Biol.*, **24**, 132–140.

28. Tomecki,R., Kristiansen,M.S., Lykke-Andersen,S., Chlebowski,A., Larsen,K.M., Szczesny,R.J., Drazkowska,K., Pastula,A., Andersen,J.S., Stepien,P.P., *et al.* (2010) The human core exosome interacts with differentially localized processive RNases: hDIS3 and hDIS3L. *EMBO J.*, **29**, 2342–2357.

29. Shiomi,T., Fukushima,K., Suzuki,N., Nakashima,N., Noguchi,E. and Nishimoto,T. (1998) Human dis3p, which binds to either GTP- or GDP-Ran, complements Saccharomyces cerevisiae dis3. *J. Biochem. (Tokyo)*, **123**, 883–890.

30. Tomecki,R. and Dziembowski,A. (2010) Novel endoribonucleases as central players in various pathways of eukaryotic RNA metabolism. *RNA*, **16**, 1692–1724.

31. Houseley,J. and Tollervey,D. (2009) The many pathways of RNA degradation. *Cell*, **136**, 763–776.

32. Lee,N.N., Chalamcharla,V.R., Reyes-Turcu,F., Mehta,S., Zofall,M., Balachandran,V., Dhakshnamoorthy,J., Taneja,N., Yamanaka,S., Zhou,M., *et al.* (2013) Mtr4-like Protein Coordinates Nuclear RNA Processing for Heterochromatin Assembly and for Telomere Maintenance. *Cell*, **155**, 1061–1074.

33. Weick,E.-M., Puno,M.R., Januszyk,K., Zinder,J.C., DiMattia,M.A. and Lima,C.D. (2018) Helicase-Dependent RNA Decay Illuminated by a Cryo-EM Structure of a Human Nuclear RNA Exosome-MTR4 Complex. *Cell*, **173**, 1663-1677.e21.

34. Falk,S., Bonneau,F., Ebert,J., Kögel,A. and Conti,E. (2017) Mpp6 Incorporation in the Nuclear Exosome Contributes to RNA Channeling through the Mtr4 Helicase. *Cell Rep.*, **20**, 2279–2286.

35. Vanácová,S., Wolf,J., Martin,G., Blank,D., Dettwiler,S., Friedlein,A., Langen,H., Keith,G. and Keller,W. (2005) A new yeast poly(A) polymerase complex involved in RNA quality control. *PLoS Biol.*, **3**, e189.

36. LaCava,J., Houseley,J., Saveanu,C., Petfalski,E., Thompson,E., Jacquier,A. and Tollervey,D. (2005) RNA Degradation by the Exosome Is Promoted by a Nuclear Polyadenylation Complex. *Cell*, **121**, 713–724.

37. Bühler,M., Spies,N., Bartel,D.P. and Moazed,D. (2008) TRAMP-mediated RNA surveillance prevents spurious entry of RNAs into the Schizosaccharomyces pombe siRNA pathway. *Nat. Struct. Mol. Biol.*, **15**, 1015–1023.

38. Vasiljeva,L., Kim,M., Mutschler,H., Buratowski,S. and Meinhart,A. (2008) The Nrd1-Nab3-Sen1 termination complex interacts with the Ser5-phosphorylated RNA polymerase II C-terminal domain. *Nat. Struct. Mol. Biol.*, **15**, 795–804.

39. Vasiljeva,L. and Buratowski,S. (2006) Nrd1 interacts with the nuclear exosome for 3' processing of RNA polymerase II transcripts. *Mol. Cell*, **21**, 239–248.

40. Tudek,A., Porrua,O., Kabzinski,T., Lidschreiber,M., Kubicek,K., Fortova,A., Lacroute,F., Vanacova,S., Cramer,P., Stefl,R., *et al.* (2014) Molecular basis for coordinating transcription termination with noncoding RNA degradation. *Mol. Cell*, **55**, 467–481.

41. Thiebaut,M., Kisseleva-Romanova,E., Rougemaille,M., Boulay,J. and Libri,D. (2006) Transcription termination and nuclear degradation of cryptic unstable transcripts: a role for the nrd1-nab3 pathway in genome surveillance. *Mol. Cell*, **23**, 853–864.

42. Egan,E.D., Braun,C.R., Gygi,S.P. and Moazed,D. (2014) Post-transcriptional regulation of meiotic genes by a nuclear RNA silencing complex. *RNA N. Y. N*, **20**, 867–881.

43. Sugiyama,T. and Sugioka-Sugiyama,R. (2011) Red1 promotes the elimination of meiosis-specific mRNAs in vegetatively growing fission yeast. *EMBO J.*, **30**, 1027–1039.

44. Yamashita,A., Takayama,T., Iwata,R. and Yamamoto,M. (2013) A novel factor Iss10 regulates Mmi1-mediated selective elimination of meiotic transcripts. *Nucleic Acids Res.*, **41**, 9680–9687.

45. Yamashita,A., Shichino,Y., Tanaka,H., Hiriart,E., Touat-Todeschini,L., Vavasseur,A., Ding,D.-Q., Hiraoka,Y., Verdel,A. and Yamamoto,M. (2012) Hexanucleotide motifs mediate recruitment of the RNA elimination machinery to silent meiotic genes. *Open Biol.*, **2**, 120014.

46. Vo,T.V., Dhakshnamoorthy,J., Larkin,M., Zofall,M., Thillainadesan,G., Balachandran,V., Holla,S.,

Wheeler,D. and Grewal,S.I.S. (2019) CPF Recruitment to Non-canonical Transcription Termination Sites Triggers Heterochromatin Assembly and Gene Silencing. *Cell Rep.*, **28**, 267-281.e5.

47. Ohkura,H., Adachi,Y., Kinoshita,N., Niwa,O., Toda,T. and Yanagida,M. (1988) Cold-sensitive and caffeine-supersensitive mutants of the Schizosaccharomyces pombe dis genes implicated in sister chromatid separation during mitosis. *EMBO J.*, **7**, 1465–1473.

48. Murakami,H., Goto,D.B., Toda,T., Chen,E.S., Grewal,S.I., Martienssen,R.A. and Yanagida,M. (2007) Ribonuclease Activity of Dis3 Is Required for Mitotic Progression and Provides a Possible Link between Heterochromatin and Kinetochore Function. *PLOS ONE*, **2**, e317.

49. Kilchert,C., Kecman,T., Priest,E., Hester,S., Aydin,E., Kus,K., Rossbach,O., Castello,A., Mohammed,S. and Vasiljeva,L. (2020) System-wide analyses of the fission yeast poly(A)+ RNA interactome reveal insights into organization and function of RNA-protein complexes. *Genome Res.*, 10.1101/gr.257006.119.

50. Garcia-Moreno,M., Noerenberg,M., Ni,S., Järvelin,A.I., González-Almela,E., Lenz,C.E., Bach-Pages,M., Cox,V., Avolio,R., Davis,T., *et al.* (2019) System-wide Profiling of RNA-Binding Proteins Uncovers Key Regulators of Virus Infection. *Mol. Cell*, **74**, 196-211.e11.

51. Paul,B. and Montpetit,B. (2016) Altered RNA processing and export lead to retention of mRNAs near transcription sites and nuclear pore complexes or within the nucleolus. *Mol. Biol. Cell*, **27**, 2742–2756.

52. Fan,J., Kuai,B., Wu,G., Wu,X., Chi,B., Wang,L., Wang,K., Shi,Z., Zhang,H., Chen,S., *et al.* (2017) Exosome cofactor hMTR4 competes with export adaptor ALYREF to ensure balanced nuclear RNA pools for degradation and export. *EMBO J.*, **36**, 2870–2886.

53. Silla,T., Karadoulama,E., Mąkosa,D., Lubas,M. and Jensen,T.H. (2018) The RNA Exosome Adaptor ZFC3H1 Functionally Competes with Nuclear Export Activity to Retain Target Transcripts. *Cell Rep.*, **23**, 2199–2210.

54. Lunde,B.M., Moore,C. and Varani,G. (2007) RNA-binding proteins: modular design for efficient function. *Nat. Rev. Mol. Cell Biol.*, **8**, 479–490.

55. Bühler,M., Haas,W., Gygi,S.P. and Moazed,D. (2007) RNAi-dependent and -independent RNA turnover mechanisms contribute to heterochromatic gene silencing. *Cell*, **129**, 707–721.

56. Telekawa,C., Boisvert,F.-M. and Bachand,F. (2018) Proteomic profiling and functional characterization of post-translational modifications of the fission yeast RNA exosome. *Nucleic Acids Res.*, **46**, 11169–11183.

57. Bitton,D.A., Schubert,F., Dey,S., Okoniewski,M., Smith,G.C., Khadayate,S., Pancaldi,V., Wood,V. and Bähler,J. (2015) AnGeLi: A Tool for the Analysis of Gene Lists from Fission Yeast. *Front. Genet.*, **6**.

58. Hirose,M., Tohda,H., Giga-Hama,Y., Tsushima,R., Zako,T., Iizuka,R., Pack,C., Kinjo,M., Ishii,N. and Yohda,M. (2005) Interaction of a small heat shock protein of the fission yeast, Schizosaccharomyces pombe, with a denatured protein at elevated temperature. *J. Biol. Chem.*, **280**, 32586–32593.

59. Lemay,J.-F., D'Amours,A., Lemieux,C., Lackner,D.H., St-Sauveur,V.G., Bähler,J. and Bachand,F. (2010) The nuclear poly(A)-binding protein interacts with the exosome to promote synthesis of noncoding small nucleolar RNAs. *Mol. Cell*, **37**, 34–45.

60. Massenet,S., Bertrand,E. and Verheggen,C. (2017) Assembly and trafficking of box C/D and

H/ACA snoRNPs. *RNA Biol.*, **14**, 680–692.

61. Darzacq,X., Kittur,N., Roy,S., Shav-Tal,Y., Singer,R.H. and Meier,U.T. (2006) Stepwise RNP assembly at the site of H/ACA RNA transcription in human cells. *J. Cell Biol.*, **173**, 207–218.

62. Li,S., Duan,J., Li,D., Yang,B., Dong,M. and Ye,K. (2011) Reconstitution and structural analysis of the yeast box H/ACA RNA-guided pseudouridine synthase. *Genes Dev.*, **25**, 2409–2421.

63. Wilkinson,M.E., Charenton,C. and Nagai,K. (2020) RNA Splicing by the Spliceosome. *Annu. Rev. Biochem.*, **89**, null.

64. Bresson,S.M. and Conrad,N.K. (2013) The human nuclear poly(a)-binding protein promotes RNA hyperadenylation and decay. *PLoS Genet.*, **9**, e1003893.

65. Yamanaka,S., Yamashita,A., Harigaya,Y., Iwata,R. and Yamamoto,M. (2010) Importance of polyadenylation in the selective elimination of meiotic mRNAs in growing S. pombe cells. *EMBO J.*, **29**, 2173–2181.

66. Proudfoot,N.J. (2011) Ending the message: poly(A) signals then and now. *Genes Dev.*, **25**, 1770–1782.

67. Thore,S. and Fribourg,S. (2019) Structural insights into the 3′-end mRNA maturation machinery: Snapshot on polyadenylation signal recognition. *Biochimie*, **164**, 105–110.

68. Win,T.Z., Draper,S., Read,R.L., Pearce,J., Norbury,C.J. and Wang,S.-W. (2006) Requirement of fission yeast Cid14 in polyadenylation of rRNAs. *Mol. Cell. Biol.*, **26**, 1710–1721.

69. Wittmann,S., Renner,M., Watts,B.R., Adams,O., Huseyin,M., Baejen,C., El Omari,K., Kilchert,C., Heo,D.-H., Kecman,T., *et al.* (2017) The conserved protein Seb1 drives transcription termination by binding RNA polymerase II and nascent RNA. *Nat. Commun.*, **8**, 14861.

70. Lemay,J.-F., Marguerat,S., Larochelle,M., Liu,X., van Nues,R., Hunyadkürti,J., Hoque,M., Tian,B., Granneman,S., Bähler,J., *et al.* (2016) The Nrd1-like protein Seb1 coordinates cotranscriptional 3' end processing and polyadenylation site selection. *Genes Dev.*, **30**, 1558–1572.

71. Wang,C., Liu,Y., DeMario,S.M., Mandric,I., Gonzalez-Figueroa,C. and Chanfreau,G.F. (2020) Rrp6 Moonlights in an RNA Exosome-Independent Manner to Promote Cell Survival and Gene Expression during Stress. *Cell Rep.*, **31**, 107754.

72. Andrulis,E.D., Werner,J., Nazarian,A., Erdjument-Bromage,H., Tempst,P. and Lis,J.T. (2002) The RNA processing exosome is linked to elongating RNA polymerase II in Drosophila. *Nature*, **420**, 837–841.

73. Ard,R., Tong,P. and Allshire,R.C. (2014) Long non-coding RNA-mediated transcriptional interference of a permease gene confers drug tolerance in fission yeast. *Nat. Commun.*, **5**, 5576.

74. Lloret-Llinares,M., Karadoulama,E., Chen,Y., Wojenski,L.A., Villafano,G.J., Bornholdt,J., Andersson,R., Core,L., Sandelin,A. and Jensen,T.H. (2018) The RNA exosome contributes to gene expression regulation during stem cell differentiation. *Nucleic Acids Res.*, **46**, 11502–11513.

75. Blasius,M., Wagner,S.A., Choudhary,C., Bartek,J. and Jackson,S.P. (2014) A quantitative 14-3-3 interaction screen connects the nuclear exosome targeting complex to the DNA damage response. *Genes Dev.*, **28**, 1977–1982.

76. Marin-Vicente,C., Domingo-Prim,J., Eberle,A.B. and Visa,N. (2015) RRP6/EXOSC10 is required for the repair of DNA double-strand breaks by homologous recombination. *J. Cell Sci.*, **128**, 1097–

1107.

77. Keller,C., Woolcock,K., Hess,D. and Bühler,M. (2010) Proteomic and functional analysis of the noncanonical poly(A) polymerase Cid14. *RNA*, **16**, 1124–1129.

78. Sugiyama,T., Wanatabe,N., Kitahata,E., Tani,T. and Sugioka-Sugiyama,R. (2013) Red5 and three nuclear pore components are essential for efficient suppression of specific mRNAs during vegetative growth of fission yeast. *Nucleic Acids Res.*, **41**, 6674–6686.

79. Fasken,M.B., Leung,S.W., Banerjee,A., Kodani,M.O., Chavez,R., Bowman,E.A., Purohit,M.K., Rubinson,M.E., Rubinson,E.H. and Corbett,A.H. (2011) Air1 Zinc Knuckles 4 and 5 and a Conserved IWRXY Motif Are Critical for the Function and Integrity of the Trf4/5-Air1/2-Mtr4 Polyadenylation (TRAMP) RNA Quality Control Complex. *J. Biol. Chem.*, **286**, 37429–37445.

80. Winczura,K., Schmid,M., Iasillo,C., Molloy,K.R., Harder,L.M., Andersen,J.S., LaCava,J. and Jensen,T.H. (2018) Characterizing ZC3H18, a Multi-domain Protein at the Interface of RNA Production and Destruction Decisions. *Cell Rep.*, **22**, 44–58.

81. Lubas,M., Christensen,M.S., Kristiansen,M.S., Domanski,M., Falkenby,L.G., Lykke-Andersen,S., Andersen,J.S., Dziembowski,A. and Jensen,T.H. (2011) Interaction Profiling Identifies the Human Nuclear Exosome Targeting Complex. *Mol. Cell*, **43**, 624–637.

82. Meola,N., Domanski,M., Karadoulama,E., Chen,Y., Gentil,C., Pultz,D., Vitting-Seerup,K., Lykke-Andersen,S., Andersen,J.S., Sandelin,A., *et al.* (2016) Identification of a Nuclear Exosome Decay Pathway for Processed Transcripts. *Mol. Cell*, **64**, 520–533.

83. Gustafson,M.P., Welcker,M., Hwang,H.C. and Clurman,B.E. (2005) Zcchc8 is a glycogen synthase kinase-3 substrate that interacts with RNA-binding proteins. *Biochem. Biophys. Res. Commun.*, **338**, 1359–1367.

84. Ogami,K., Richard,P., Chen,Y., Hoque,M., Li,W., Moresco,J.J., Yates,J.R., Tian,B. and Manley,J.L. (2017) An Mtr4/ZFC3H1 complex facilitates turnover of unstable nuclear RNAs to prevent their cytoplasmic transport and global translational repression. *Genes Dev.*, **31**, 1257–1271.

85. Silla,T., Schmid,M., Dou,Y., Garland,W., Milek,M., Imami,K., Johnsen,D., Polak,P., Andersen,J.S., Selbach,M., *et al.* (2020) The human ZC3H3 and RBM26/27 proteins are critical for PAXT-mediated nuclear RNA decay. *Nucleic Acids Res.*, **48**, 2518–2530.

86. Lingaraju,M., Johnsen,D., Schlundt,A., Langer,L.M., Basquin,J., Sattler,M., Jensen,T.H., Falk,S. and Conti,E. (2019) The MTR4 helicase recruits nuclear adaptors of the human RNA exosome using distinct arch-interacting motifs. In *Nature Communications*.

87. Puno,M.R. and Lima,C.D. (2018) Structural basis for MTR4–ZCCHC8 interactions that stimulate the MTR4 helicase in the nuclear exosome-targeting complex. *Proc. Natl. Acad. Sci.*, **115**, E5506–E5515.

88. Thoms,M., Thomson,E., Baßler,J., Gnädig,M., Griesel,S. and Hurt,E. (2015) The Exosome Is Recruited to RNA Substrates through Specific Adaptor Proteins. *Cell*, **162**, 1029–1038.

89. Falk,S., Tants,J.-N., Basquin,J., Thoms,M., Hurt,E., Sattler,M. and Conti,E. (2017) Structural insights into the interaction of the nuclear exosome helicase Mtr4 with the preribosomal protein Nop53. *RNA N. Y. N*, **23**, 1780–1787.

90. Shichino,Y., Otsubo,Y., Yamamoto,M. and Yamashita,A. (2020) Meiotic gene silencing complex MTREC/NURS recruits the nuclear exosome to YTH-RNA-binding protein Mmi1. *PLoS Genet.*, **16**, e1008598.

91. Aronica,L., Kasparek,T., Ruchman,D., Marquez,Y., Cipak,L., Cipakova,I., Anrather,D., Mikolaskova,B., Radtke,M., Sarkar,S., *et al.* (2016) The spliceosome-associated protein Nrl1 suppresses homologous recombination-dependent R-loop formation in fission yeast. *Nucleic Acids Res.*, **44**, 1703–1717.

92. Garland,W., Comet,I., Wu,M., Radzisheuskaya,A., Rib,L., Vitting-Seerup,K., Lloret-Llinares,M., Sandelin,A., Helin,K. and Jensen,T.H. (2019) A Functional Link between Nuclear RNA Decay and Transcriptional Control Mediated by the Polycomb Repressive Complex 2. *Cell Rep.*, **29**, 1800-1811.e6.

93. Moreno,S., Klar,A. and Nurse,P. (1991) Molecular genetic analysis of fission yeast Schizosaccharomyces pombe. *Methods Enzymol.*, **194**, 795–823.

94. Bähler,J., Wu,J.Q., Longtine,M.S., Shah,N.G., McKenzie,A., Steever,A.B., Wach,A., Philippsen,P. and Pringle,J.R. (1998) Heterologous modules for efficient and versatile PCR-based gene targeting in Schizosaccharomyces pombe. *Yeast Chichester Engl.*, **14**, 943–951.

95. Feytout,A., Vaur,S., Genier,S., Vazquez,S. and Javerzat,J.-P. (2011) Psm3 acetylation on conserved lysine residues is dispensable for viability in fission yeast but contributes to Eso1-mediated sister chromatid cohesion by antagonizing Wpl1. *Mol. Cell. Biol.*, **31**, 1771–1786.

96. Birot,A., Tormos-Pérez,M., Vaur,S., Feytout,A., Jaegy,J., Alonso Gil,D., Vazquez,S., Ekwall,K. and Javerzat,J.-P. (2020) The CDK Pef1 and protein phosphatase 4 oppose each other for regulating cohesin binding to fission yeast chromosomes. *eLife*, **9**.

97. Kilchert,C., Hester,S., Castello,A., Mohammed,S. and Vasiljeva,L. (2020) Comparative Poly(A)+ RNA Interactome Capture of RNA Surveillance Mutants. *Methods Mol. Biol. Clifton NJ*, **2062**, 255–276.

98. Zhang,X., Smits,A.H., van Tilburg,G.B., Ovaa,H., Huber,W. and Vermeulen,M. (2018) Proteome-wide identification of ubiquitin interactions using UbIA-MS. *Nat. Protoc.*, **13**, 530–550.

99. Lock,A., Rutherford,K., Harris,M.A., Hayles,J., Oliver,S.G., Bähler,J. and Wood,V. (2019) PomBase 2018: user-driven reimplementation of the fission yeast database provides rapid and intuitive access to diverse, interconnected information. *Nucleic Acids Res.*, **47**, D821–D827.

100. Heinrich,S., Sidler,C.L., Azzalin,C.M. and Weis,K. (2017) Stem–loop RNA labeling can affect nuclear and cytoplasmic mRNA processing. *RNA*, **23**, 134–141.

101. Trcek,T., Lionnet,T., Shroff,H. and Lehmann,R. (2017) mRNA quantification using single-molecule FISH in Drosophila embryos. *Nat. Protoc.*, **12**, 1326–1348.

102. Schneider,C.A., Rasband,W.S. and Eliceiri,K.W. (2012) NIH Image to ImageJ: 25 years of image analysis. *Nat. Methods*, **9**, 671–675.

103. Minvielle-Sebastia,L., Winsor,B., Bonneaud,N. and Lacroute,F. (1991) Mutations in the yeast RNA14 and RNA15 genes result in an abnormal mRNA decay rate; sequence analysis reveals an RNA-binding domain in the RNA15 protein. *Mol. Cell. Biol.*, **11**, 3075–3087.

104. Langmead,B. and Salzberg,S.L. (2012) Fast gapped-read alignment with Bowtie 2. *Nat. Methods*, **9**, 357–359.

105. Li,H., Handsaker,B., Wysoker,A., Fennell,T., Ruan,J., Homer,N., Marth,G., Abecasis,G., Durbin,R. and 1000 Genome Project Data Processing Subgroup (2009) The Sequence Alignment/Map format and SAMtools. *Bioinforma. Oxf. Engl.*, **25**, 2078–2079.

106. Eser,P., Wachutka,L., Maier,K.C., Demel,C., Boroni,M., Iyer,S., Cramer,P. and Gagneur,J. (2016) Determinants of RNA metabolism in the Schizosaccharomyces pombe genome. *Mol. Syst. Biol.*, **12**.

107. Love,M.I., Huber,W. and Anders,S. (2014) Moderated estimation of fold change and dispersion for RNA-seq data with DESeq2. *Genome Biol.*, **15**, 550.

FIGURE LEGENDS

Figure 1: Comparative poly(A)+ RNA interactome capture from fission yeast exosome mutants. A. Schematic diagram describing domain organisation of *S. pombe* (Sp) Dis3 and Mtl1 and position of the mutations in *dis3-54* (P509L) and *mtl1-1* (I522M, L543P, Y551H, L557P, D793G, A998V) shown in yellow. **B.** Schematic diagram describing the poly(A)+ interactome capture approach. Cells were grown in the presence of 4-thiouracil (4sU) and exposed to UV (3J/cm_2) to allow protein-RNA crosslinking. Poly(A)+ RNA and associated proteins were pulled down by oligo-d(T) beads and subjected to RNA sequencing and mass spectrometry analyses (RBP= RNA-Binding Proteins, EF = Exosome Factors, involved in recognition of the exosome substrates such as Mmi1). **C**. Volcano plots showing distribution of Mmi1 enrichment on poly(A)+ RNA in the three exosome mutants. In the volcano plot, *p*-values (-log10, moderated Student's t-test) are plotted against the ratio of log2-fold changes in mass spectrometry (MS) intensities for the whole-cell extract normalised proteomes of mutants versus WT cells recovered from the oligo-d(T) pull-downs of UV-crosslinked samples (3 J/cm_2). In all panels, individual proteins are depicted as a single dot. **D**. Heat map analysis of poly(A)+ RNA-seq showing differential expression of the Mmi1 regulon in exosome mutants compared to WT.

Figure 2: Rrp6 and Mtl1 are functionally linked. A. mRNAs and ncRNAs are up-regulated (>1.5-fold, *p*-value<0.05) in *mtl1-1*, *rrp6Δ* and *dis3-54* mutants compared to WT. **B.** Venn diagram showing overlap between RNAs that show increased levels (>1.5-fold, *p*-value<0.05) in *mtl1-1*, *rrp6Δ* and *dis3-54*. The *p*-values indicate the probabilities that the observed overlaps occurred by chance (6949 genes analysed). **C.** Venn diagram showing proteins commonly enriched in poly(A)+ RNA pull-down of *mtl1-1* and either *rrp6Δ* or *dis3-54* relative to WT. The *p*-values indicate the probabilities that the observed overlaps occurred by chance (6949 genes analysed). **D**. Venn diagram showing proteins depleted in poly(A)+ pull-down of *mtl1-1* and either *rrp6Δ* or *dis3-54* relative to WT. The *p*-values indicate the probabilities that the observed overlaps occurred by chance (1146 proteins analysed). **E**. RNA association of nuclear proteins is primarily affected in the exosome mutants (GO:0005575). **F**. Poly(A)+ RNA FISH illustrating accumulation of poly(A)+ RNA in the nucleus in *rrp6Δ* mutant. DAPI is shown in blue. Poly(A)+ RNA is visualised in green. Scale bar = 5µm.

Supplementary Figure S1: A. Venn diagram showing overlap between mRNAs increased levels in *mtl1-1*, *rrp6Δ* and *dis3-54* mutants compared to WT (>1.5-fold, *p*-value<0.05). The *p*-values indicate the probabilities that the observed overlaps occurred by chance (5153 mRNAs analysed). **B**. Venn diagram showing overlap between ncRNAs that show increased levels in *mtl1-1*, *rrp6Δ* and *dis3-54*

mutants compared to WT (>1.5-fold, *p*-value<0.05). The *p*-values indicate the probabilities that the observed overlaps occurred by chance (1796 ncRNAs analysed). **C-D.** Poly(A)+ RNA FISH illustrating poly(A)+ RNA accumulation in the nucleus in *mtl1-1* (**C**) and *dis3-54* (**D**). DAPI is shown in blue. Poly(A)+ RNA is represented in green. Scale bar = 5µm.

Figure 3: Comparative RIC uncovers putative novel exosome factors. **A.** List of the candidate proteins enriched on poly(A)+ RNA in the exosome mutants, their predicted function and volcano plot showing their distribution in *mtl1-1*, *rrp6Δ* and *dis3-54* mutants. **B.** Analyses of *tf2-1* mRNA levels by northern blot in the indicated strains. Band corresponding to *tf2-1* is indicated with an arrow. Schematics shows location of the probe with a black bar. The *adh1* mRNA is used as a loading control. **C.** Poly(A)+ RNA FISH illustrating cellular localisation of poly(A)+ RNA in the indicated strains. DAPI is shown in blue. Poly(A)+ RNA is visualised in green. Scale bar = 10µm. **D.** Serial dilutions of the indicated strains plated on complete medium supplemented with adenine (YES+A), medium lacking uracil (-URA) and containing 5-FOA (5-FOA) and grown at 25°C. A schematic representation of the Chromosome I (Chr I) depicting centromeric and telomeric regions (grey circle and grey rectangles correspondently). Position of where *ura4*+ reporter integrated into the left arm of the telomere is shown.

Supplementary Figure S2: A. Poly(A)+ RNA FISH illustrating poly(A)+ RNA location in the indicated strains. DAPI is shown in blue. Poly(A)+ RNA is visualised in green. Scale bar = 10µm. **B.** Serial dilutions of the indicated strains plated on complete medium (YES+A), lacking uracil (-URA) and containing 5-FOA (5-FOA) at 30°C. Related to Figure 3D.

Figure 4: The uncharacterised fission yeast protein Mub1 is a new exosome regulatory factor. A. Venn diagram showing overlap between RNAs that show an increase in levels in *mtl1-1* and *mub1Δ* (>1.5-fold, *p*-value<0.05) **B.** Genome browser snapshots showing RNA-seq data and northern blot analyses for two representative transcripts (*gst2* and *spcc663.08c*) upregulated in *mtl1-1* and *mub1Δ* compared to WT. Bands corresponding to *gst2* and *spcc663.08c* are indicated with arrows. Positions of the probes are indicated with black bars. 28S ribosomal RNAs (rRNA) visualised with methylene blue served as the loading control **C.** Co-immunoprecipitation of Rrp6-Myc with Mub1-3xFLAG**. D.** Graphical representation of WT Mub1 and Mub1-Δ-Zinc-Finger. **E.** Western blot showing levels of endogenously expressed Mub1-3xFLAG and Mub1-ΔZ-3xFLAG proteins. **F.** Analyses of *SPCC663.08c* and *gst2* mRNAs from *mub1-3xFLAG* and *mub1-ΔZ-3xFLAG* strains by northern blot as in **B**.

Supplementary Figure S3. A. Mub1 deletion leads to altered cellular morphology. Phase contrast images of the cells from the indicated strains. Scale bar = 10µm. **B.** Serial dilutions of the indicated strains plated on complete medium (YES+A) at the indicated temperatures. **C.** Western blot showing levels of endogenously expressed Mub1-3xFLAG in WT and exosome mutants. Cellular proteins visualised with ponceau S are used to control for loading.

Figure 5: Mub1 and nuclear exosome are involved in regulation of heat shock response. A. Serial dilutions of the indicated strains plated on complete medium (YES+A) at the indicated temperatures. **B.** Analyses of *hsp16* mRNAs levels by northern blot in the indicated strains at the indicated temperatures. Band corresponding to *hsp16* mRNA is indicated with arrow. Schematic diagram shows location of the probe with a black bar. 28S ribosomal RNAs (rRNA) visualised with methylene blue served as the loading control. **C.** Serial dilutions of the indicated strains plated on complete medium (YES+A) at the indicated temperatures.

Figure 6: Rrp6 and Mtl1 are involved in H/ACA snoRNA processing. **A.** Analysis of poly(A)+ RNA-seq presented as a heat map showing differential expression of snoRNAs in the exosome mutants. Bar at the bottom of the diagram shows fold change. **B.** Genome browser snapshots showing total-RNA-seq and poly(A)+ RNA-seq data for the *snR92* locus in *mtl1-1* and WT. 3'extended part of the precursor molecule is indicated with arrows**. C.** Analyses of *snR92* and *snoR69b* by northern blot in *mtl1-1*, *rrp6Δ* and *dis3-54* exosome mutants and WT. Positions of the precursor molecules and mature RNAs are indicated with arrows. Distribution of heterogeneous poly(A)+ species of the *snR92* precursor is shown with brackets. 5.8S ribosomal RNAs (rRNA) visualised with methylene blue served as the loading control **D.** Schematic describing components of H/ACA box snoRNPs and H/ACA snRNA 3'end maturation process. **E.** Volcano plot showing distribution of H/ACA box snoRNP proteins using colour code as in Figure 3D. Proteins components of C/D box snoRNPs are shown in black. Proteins with no-significant variation are shown in clear colour.

Figure 7: Altered RNA association of mRNA processing factors in the exosome mutants. **A.** Analyses of *rps2202* levels by northern blot in *mtl1-1*, *rrp6Δ* and *dis3-54* mutants and WT. Schematics shows location of the probe with a black bar. Bands corresponding to spliced and unspliced *rps2202* are indicated with arrows. Because of high sequence conservation, the intron-less paralogue *rps2201* is also detected and indicated with an arrow. **B.** Genome browser snapshots showing poly(A)+ RNA-seq data for the *rps2202* locus in WT, *mtl1-1*, *dis3-54* and *rrp6Δ*. **C.** Schematic overview of A-complex and B* active complex of the spliceosome. Volcano plot showing enrichment of U1-U2 and decrease of NTC components in the *mtl1-1* interactome. Proteins with no-significant variation are shown in clear colour. **D**. Schematics illustrating the putative organisation of mRNA 3'end processing machinery; components of the Cleavage and Polyadenylation Factors (CPF) and Cleavage Factors (CF) IA and B. **E.** Volcano plot showing the distribution of the subunits of non-canonical poly(A) polymerase TRAMP complex and polymerase module of the CPF in *rrp6Δ* interactome*.* Proteins with no-significant variation are shown in clear colour. **F**. Volcano plot showing the distribution of the CPF components in *rrp6Δ* interactome using colour code as in D. **G.** Schematic representation of the assay measuring length of the poly(A) tails of cellular RNAs in *rrp6Δ* and WT.

Figure 8: Analysis of the poly(A)+ RNA association of the exosome related proteins in comparative RIC. A. Schematics illustrating factors known to be linked to the nuclear RNA exosome. **B.** Volcano plot showing distribution of Mmi1-Iss10, Mtl1-Red1 and exosome components in the *mtl1-1* interactome. **C.** Schematics showing a proposed model of a two-steps recruitment of the nuclear

RNA exosome to its RNA targets. I) Recognition of RNA by the RNA-binding module. II) Targeting of the exosome complex to the substrate RNA mediated by Mtl1. **D.** Volcano plot showing distribution of poly(A) binding proteins Red5, Pab2 and Rmn1 proteins in *rrp6Δ* interactome.

Figure 1

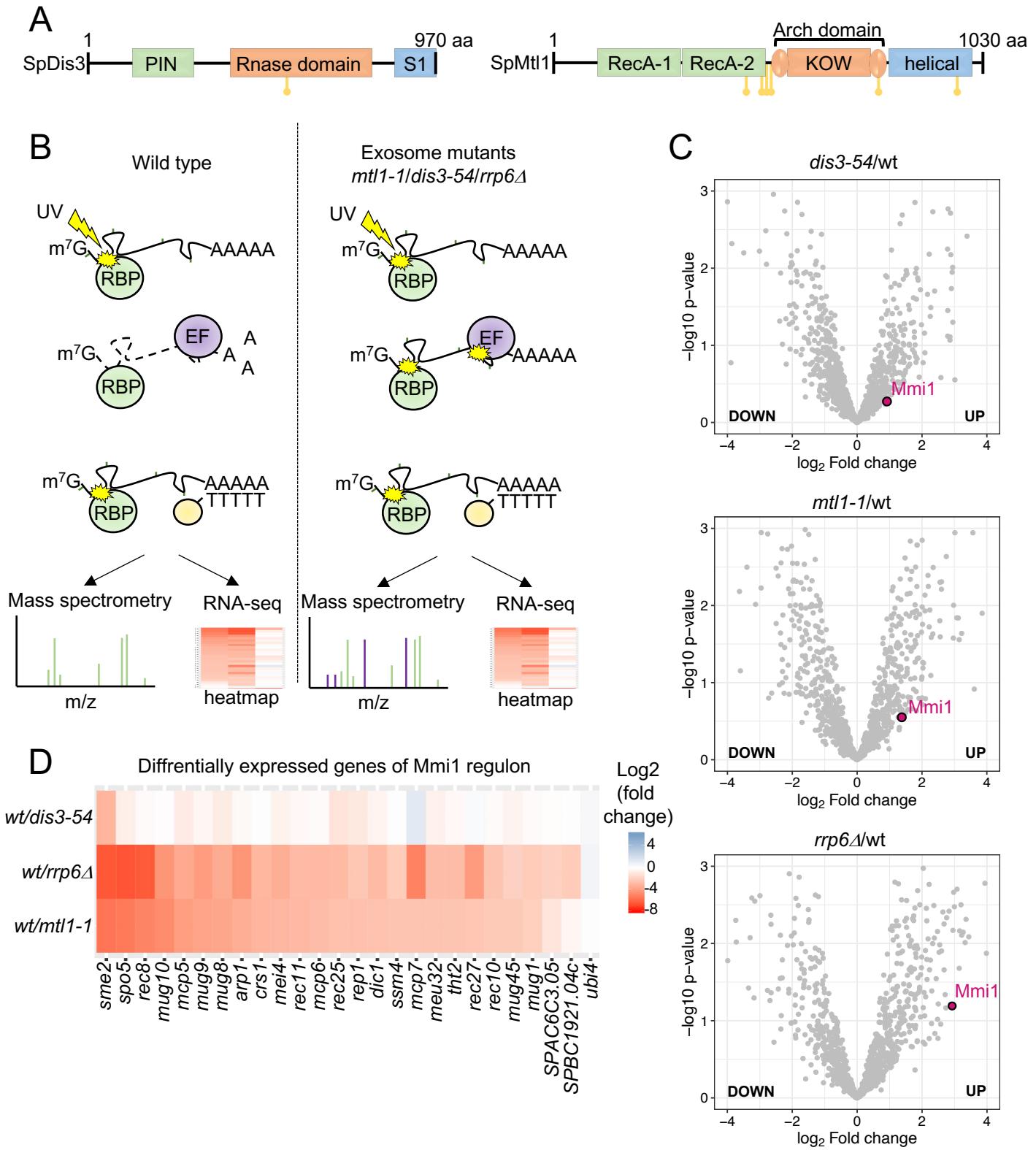
A
SpDis3
1
PIN
Rnase domain
S1
970 aa
SpMtl1
1
RecA-1
RecA-2
Arch domain
KOW
helical
1030 aa
B
Wild type
Exosome mutants
mtl1-1/dis3-54/rrp6Δ
UV
m7G
AAAAA
RBP
EF
A
TTTTT
Mass spectrometry
RNA-seq
m/z
heatmap
C
dis3-54/wt
mtl1-1/wt
rrp6Δ/wt
−log10 p−value
log2 Fold change
DOWN
UP
Mmi1
D
Diffrentially expressed genes of Mmi1 regulon
wt/dis3-54
wt/rrp6Δ
wt/mtl1-1
sme2
spo5
rec8
mug10
mcp5
mug9
mug8
arp1
crs1
mei4
rec11
mcp6
rec25
rep1
dic1
ssm4
mcp7
meu32
tht2
rec27
rec10
mug45
mug1
SPAC6C3.05
SPBC1921.04c
ubi4
Log2 (fold change)
4
0
-4
-8

Figure 2

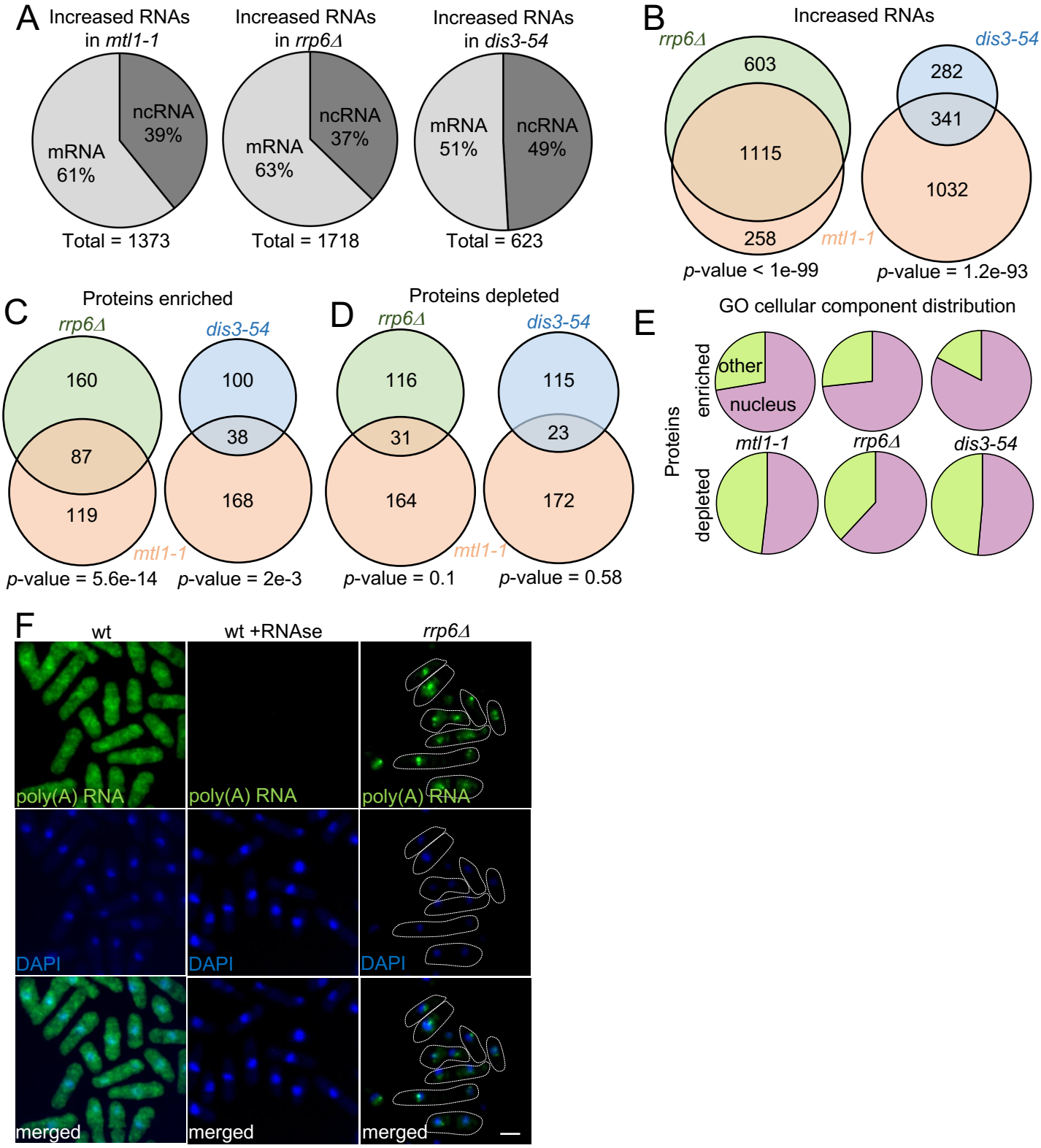
A
Increased RNAs in mtl1-1
ncRNA 39%
mRNA 61%
Total = 1373
Increased RNAs in rrp6Δ
ncRNA 37%
mRNA 63%
Total = 1718
Increased RNAs in dis3-54
mRNA 51%
ncRNA 49%
Total = 623
B
Increased RNAs
rrp6Δ
603
1115
258
mtl1-1
p-value < 1e-99
dis3-54
282
341
1032
p-value = 1.2e-93
C
Proteins enriched
rrp6Δ
160
87
119
mtl1-1
p-value = 5.6e-14
dis3-54
100
38
168
p-value = 2e-3
D
Proteins depleted
rrp6Δ
116
31
164
mtl1-1
p-value = 0.1
dis3-54
115
23
172
p-value = 0.58
E
GO cellular component distribution
Proteins
enriched
depleted
other
nucleus
mtl1-1
rrp6Δ
dis3-54
F
wt
wt +RNAse
rrp6Δ
poly(A) RNA
DAPI
merged

Supplementary Figure S1

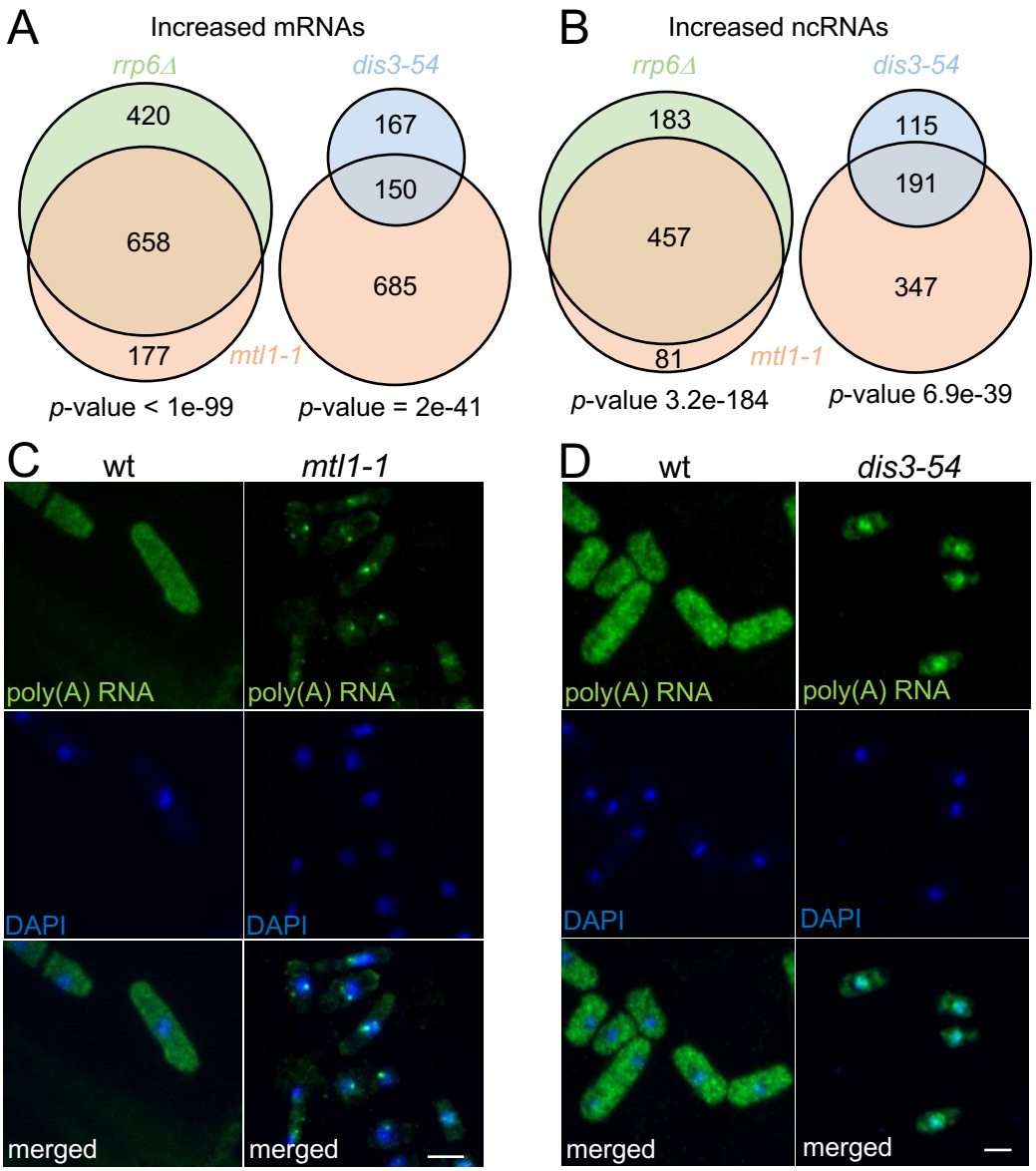

Figure 3

A

Name	Function
SPBC31F10.10c	Mub1-zf-MYND type zinc finger protein
SPBC18H10.09	zf-CHY type zinc finger protein
Swt1	RNA endoribonuclease involved in mRNP quality control Swt1 (predicted)
Pof8	F-box protein Pof8
SPAC222.18	Srp1 family splicing factor (predicted)
Srp40	SPBC1711.05 nucleocytoplasmic transport chaperone Srp40 (predicted)
SPCC126.11c	RNA-binding protein, rrm type
SPBC16G5.16	transcription factor, zf-fungal binuclear cluster type (predicted)
SPBC530.08	membrane-tethered transcription factor (predicted)
Mlo1	SPCC31H12.03c-RNA binding protein (predicted)

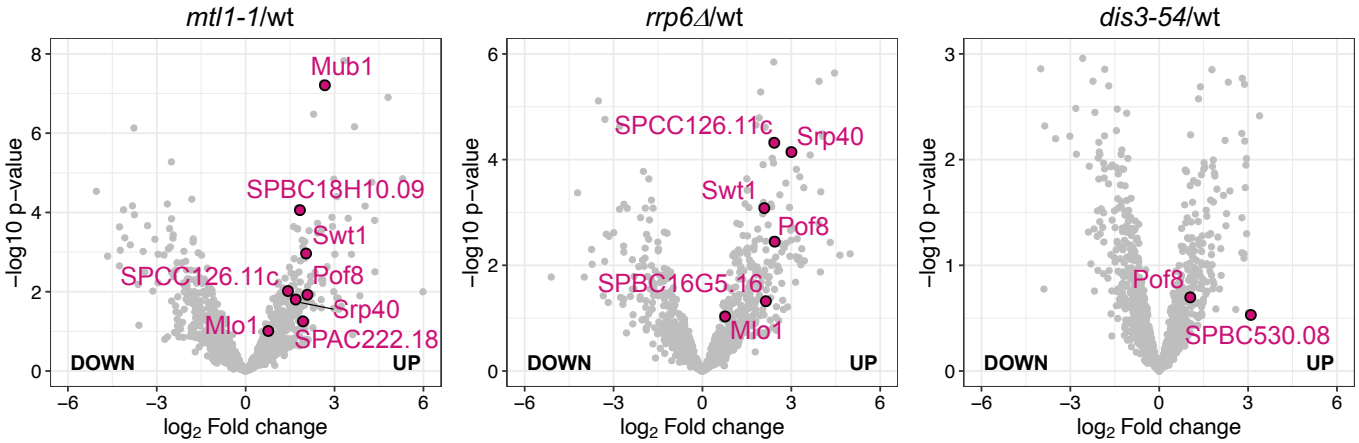

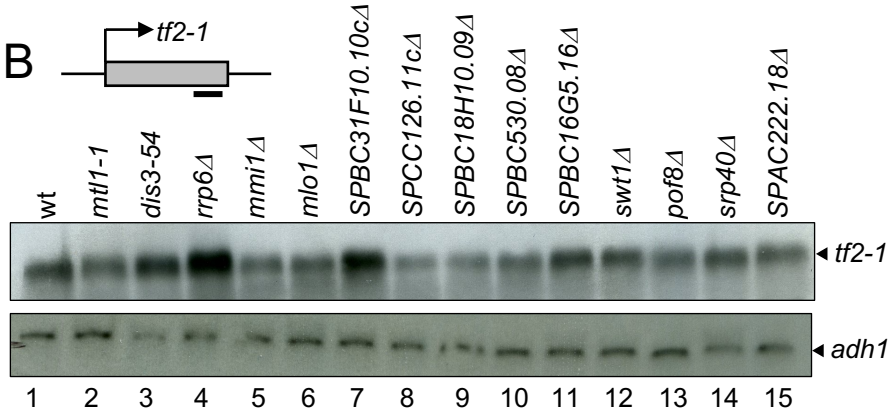

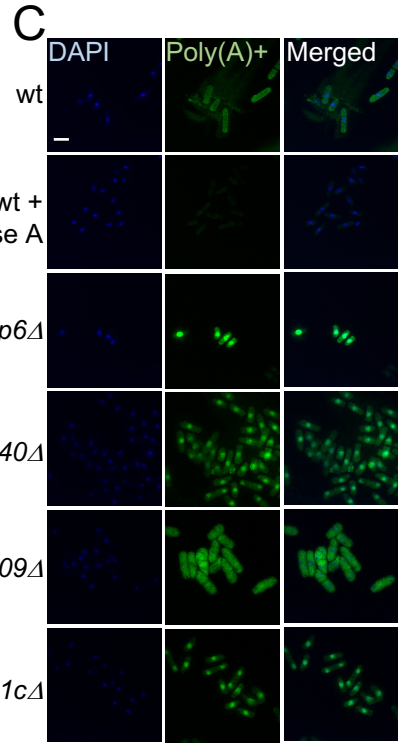

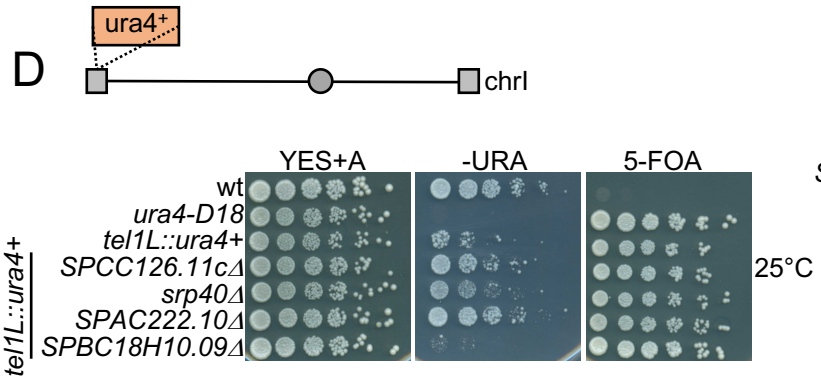

Supplementary Figure S2

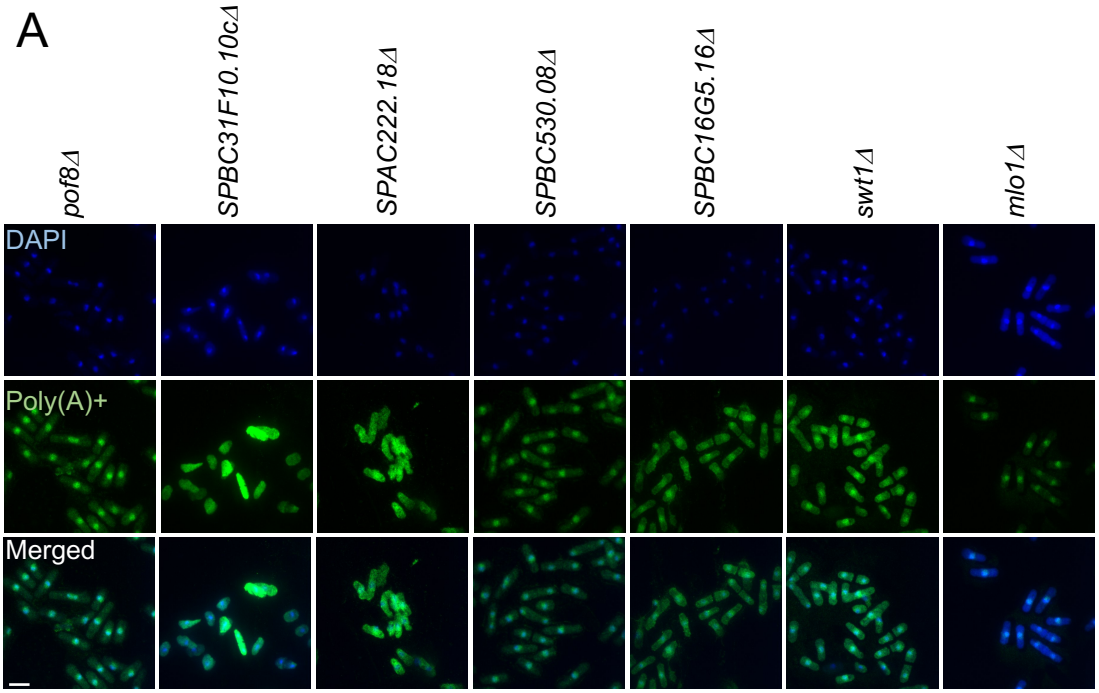

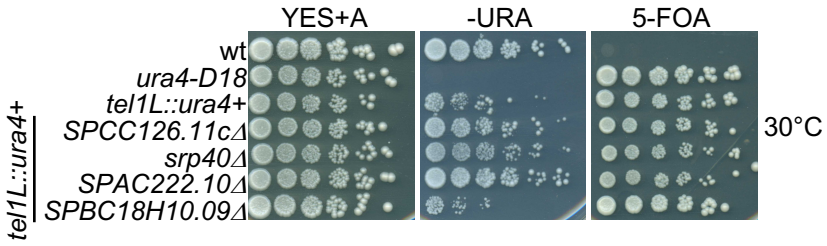

Figure 4

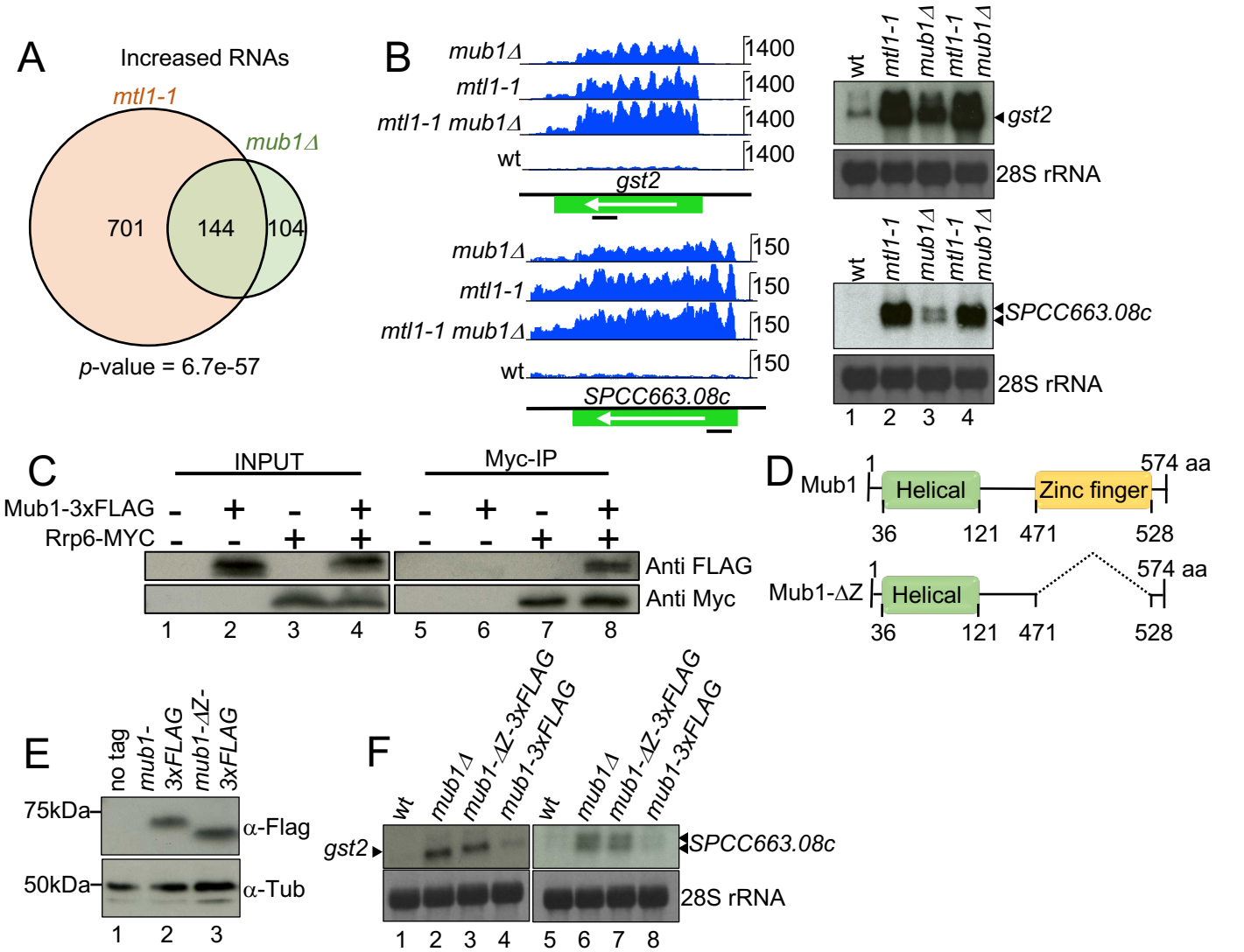
A
Increased RNAs
mtl1-1
mub1Δ
701
144
104
p-value = 6.7e-57
B
mub1Δ
mtl1-1
mtl1-1 mub1Δ
wt
1400
gst2
150
SPCC663.08c
wt
mtl1-1
mub1Δ
mtl1-1
mub1Δ
gst2
28S rRNA
SPCC663.08c
1 2 3 4
C
INPUT
Myc-IP
Mub1-3xFLAG
Rrp6-MYC
Anti FLAG
Anti Myc
1 2 3 4 5 6 7 8
D
Mub1
1
574 aa
Helical
Zinc finger
36 121 471 528
Mub1-ΔZ
E
no tag
mub1-3xFLAG
mub1-ΔZ-3xFLAG
75kDa
50kDa
α-Flag
α-Tub
1 2 3
F
wt
mub1Δ
mub1-ΔZ-3xFLAG
mub1-3xFLAG
gst2
SPCC663.08c
28S rRNA
1 2 3 4 5 6 7 8

Supplementary Figure S3

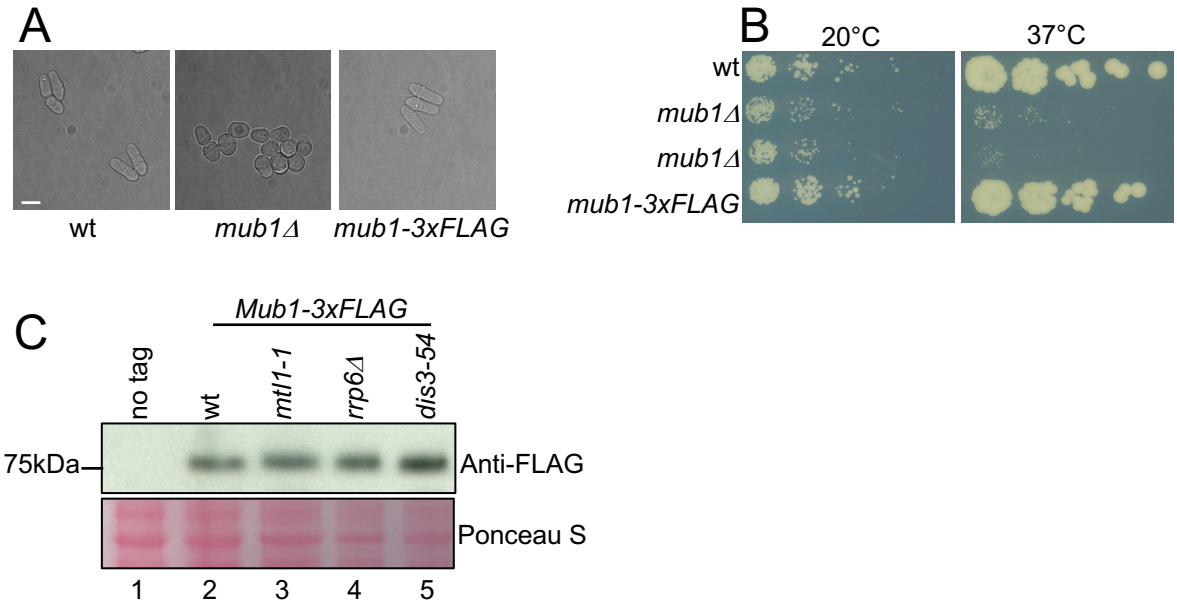

Figure 5

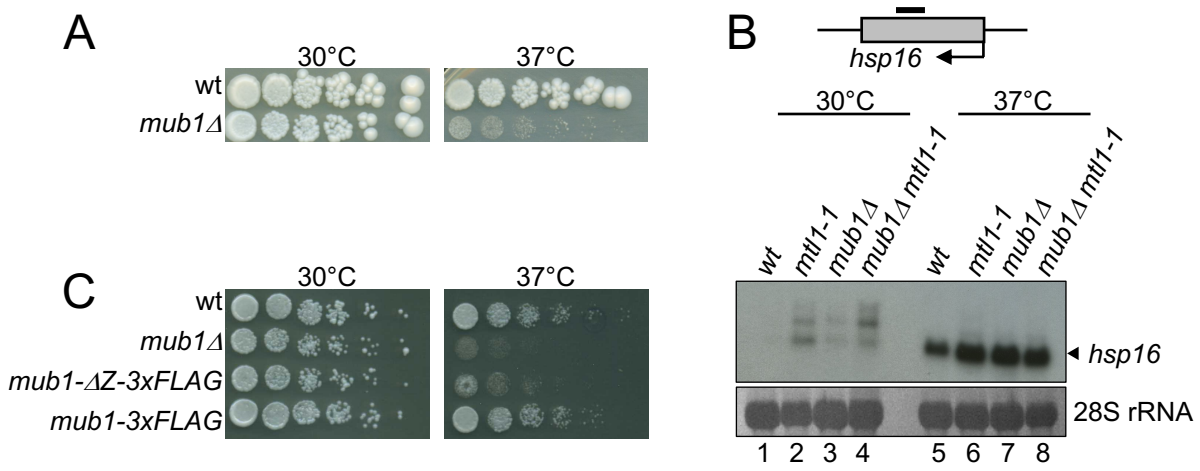
A
30°C
37°C
wt
mub1Δ
B
hsp16
30°C
37°C
wt
mtl1-1
mub1Δ
mub1Δ mtl1-1
wt
mtl1-1
mub1Δ
mub1Δ mtl1-1
hsp16
28S rRNA
1 2 3 4 5 6 7 8
C
30°C
37°C
wt
mub1Δ
mub1-ΔZ-3xFLAG
mub1-3xFLAG

Figure 6

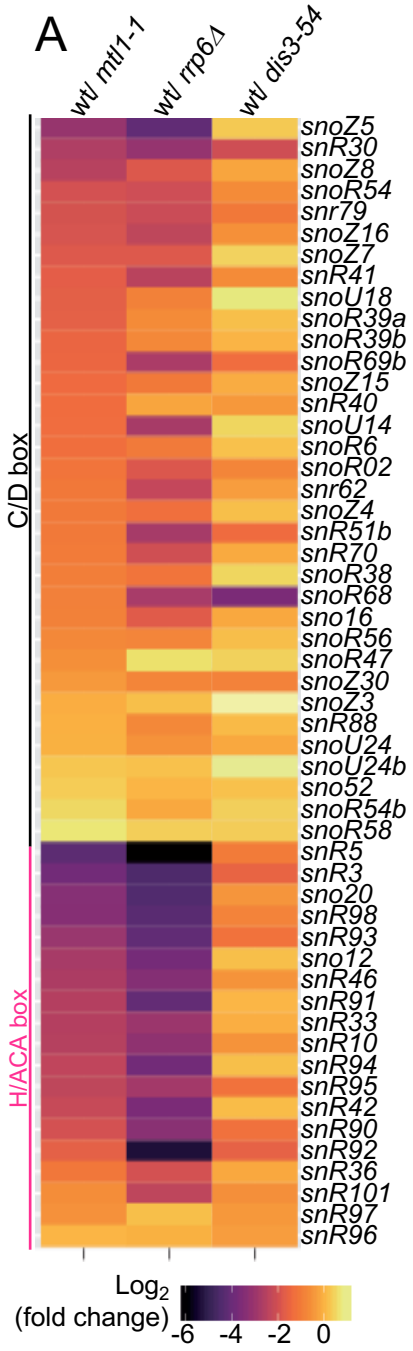
A
wt/ mtl1-1
wt/ rrp6Δ
wt/ dis3-54
C/D box
H/ACA box
snoZ5
snR30
snoZ8
snoR54
snr79
snoZ16
snoZ7
snR41
snoU18
snoR39a
snoR39b
snoR69b
snoZ15
snR40
snoU14
snoR6
snoR02
snr62
snoZ4
snR51b
snR70
snoR38
snoR68
sno16
snoR56
snoR47
snoZ30
snoZ3
snR88
snoU24
snoU24b
sno52
snoR54b
snoR58
snR5
snR3
sno20
snR98
snR93
sno12
snR46
snR91
snR33
snR10
snR94
snR95
snR42
snR90
snR92
snR36
snR101
snR97
snR96
Log2 (fold change)
-6 -4 -2 0

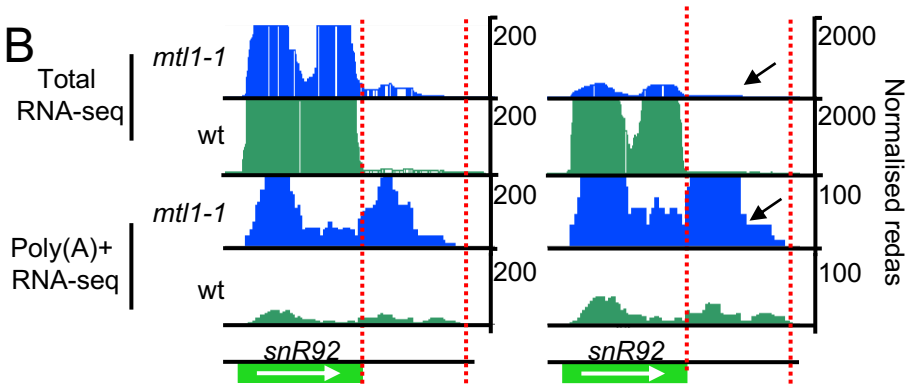
B
Total RNA-seq
Poly(A)+ RNA-seq
mtl1-1
wt
mtl1-1
wt
200
200
200
200
2000
2000
100
100
Normalised redas
snR92
snR92

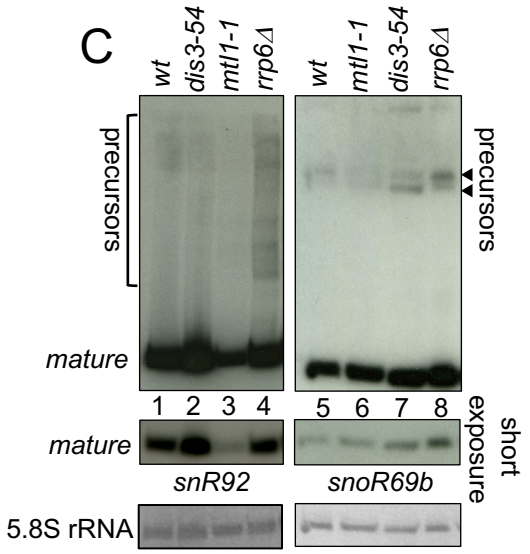
C
wt
dis3-54
mtl1-1
rrp6Δ
wt
mtl1-1
dis3-54
rrp6Δ
precursors
precursors
mature
1 2 3 4
5 6 7 8
mature
short exposure
snR92
snoR69b
5.8S rRNA

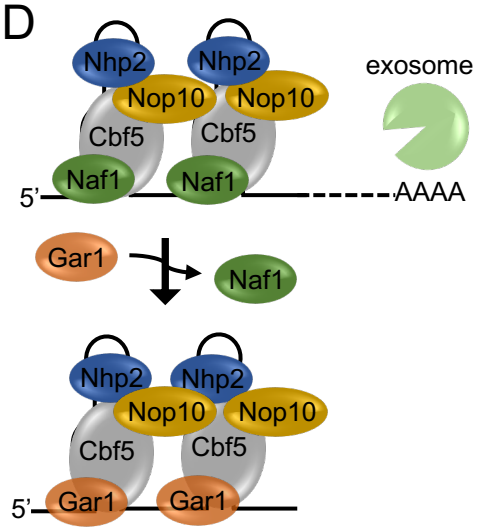
D
Nhp2
Nhp2
Nop10
Nop10
Cbf5
Cbf5
Naf1
Naf1
exosome
5'
AAAA
Gar1
Naf1
Nhp2
Nhp2
Nop10
Nop10
Cbf5
Cbf5
5'
Gar1
Gar1

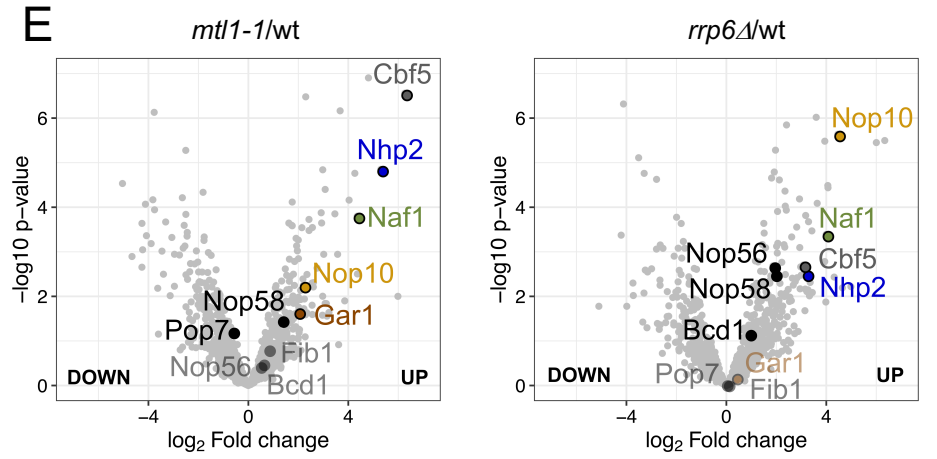
E
mtl1-1/wt
rrp6Δ/wt
−log10 p−value
log2 Fold change
DOWN
UP
Cbf5
Nhp2
Naf1
Nop10
Nop58
Gar1
Pop7
Fib1
Nop56
Bcd1
Nop10
Naf1
Nop56
Cbf5
Nop58
Nhp2
Bcd1
Gar1
Pop7
Fib1

Figure 7

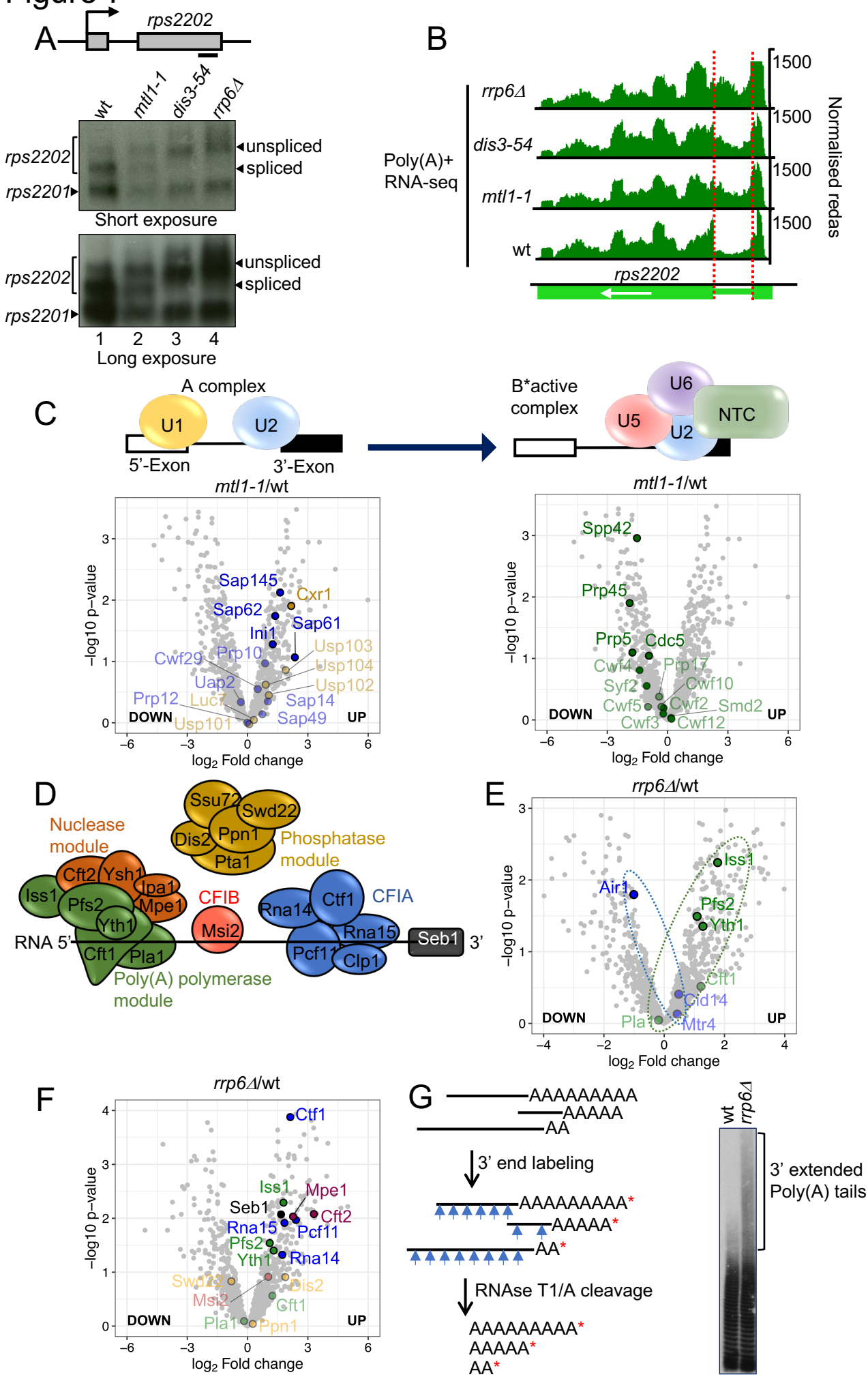
A
rps2202
wt
mtl1-1
dis3-54
rrp6Δ
rps2202
rps2201
unspliced
spliced
Short exposure
rps2202
rps2201
unspliced
spliced
1 2 3 4
Long exposure
B
rrp6Δ
dis3-54
mtl1-1
wt
Poly(A)+ RNA-seq
1500
1500
1500
1500
Normalised redas
rps2202
C
A complex
U1
U2
5'-Exon
3'-Exon
B*active complex
U6
U5
U2
NTC
mtl1-1/wt
Sap145
Cxr1
Sap62
Sap61
Ini1
Usp103
Cwf29
Prp10
Usp104
Uap2
Usp102
Prp12
Luc7
Sap14
Sap49
Usp101
DOWN
UP
−log10 p−value
log2 Fold change
mtl1-1/wt
Spp42
Prp45
Prp5
Cdc5
Cwf4
Prp17
Syf2
Cwf10
Cwf5
Cwf2
Smd2
Cwf3
Cwf12
DOWN
UP
−log10 p−value
log2 Fold change
D
Nuclease module
Ssu72
Swd22
Dis2
Ppn1
Phosphatase module
Pta1
Cft2
Ysh1
Iss1
Ipa1
Pfs2
Mpe1
Yth1
CFIB
Msi2
Rna14
Ctf1
CFIA
Rna15
RNA 5'
Cft1
Pla1
Pcf11
Clp1
Seb1
3'
Poly(A) polymerase module
E
rrp6Δ/wt
Iss1
Air1
Pfs2
Yth1
Cft1
Cid14
Pla1
Mtr4
DOWN
UP
−log10 p−value
log2 Fold change
F
rrp6Δ/wt
Ctf1
Iss1
Mpe1
Seb1
Cft2
Rna15
Pcf11
Pfs2
Yth1
Rna14
Swd22
Dis2
Msi2
Cft1
Pla1
Ppn1
DOWN
UP
−log10 p−value
log2 Fold change
G
AAAAAAAAA
AAAAA
AA
3' end labeling
AAAAAAAAA*
AAAAA*
AA*
RNAse T1/A cleavage
AAAAAAAAA*
AAAAA*
AA*
wt
rrp6Δ
3' extended Poly(A) tails

Figure 8

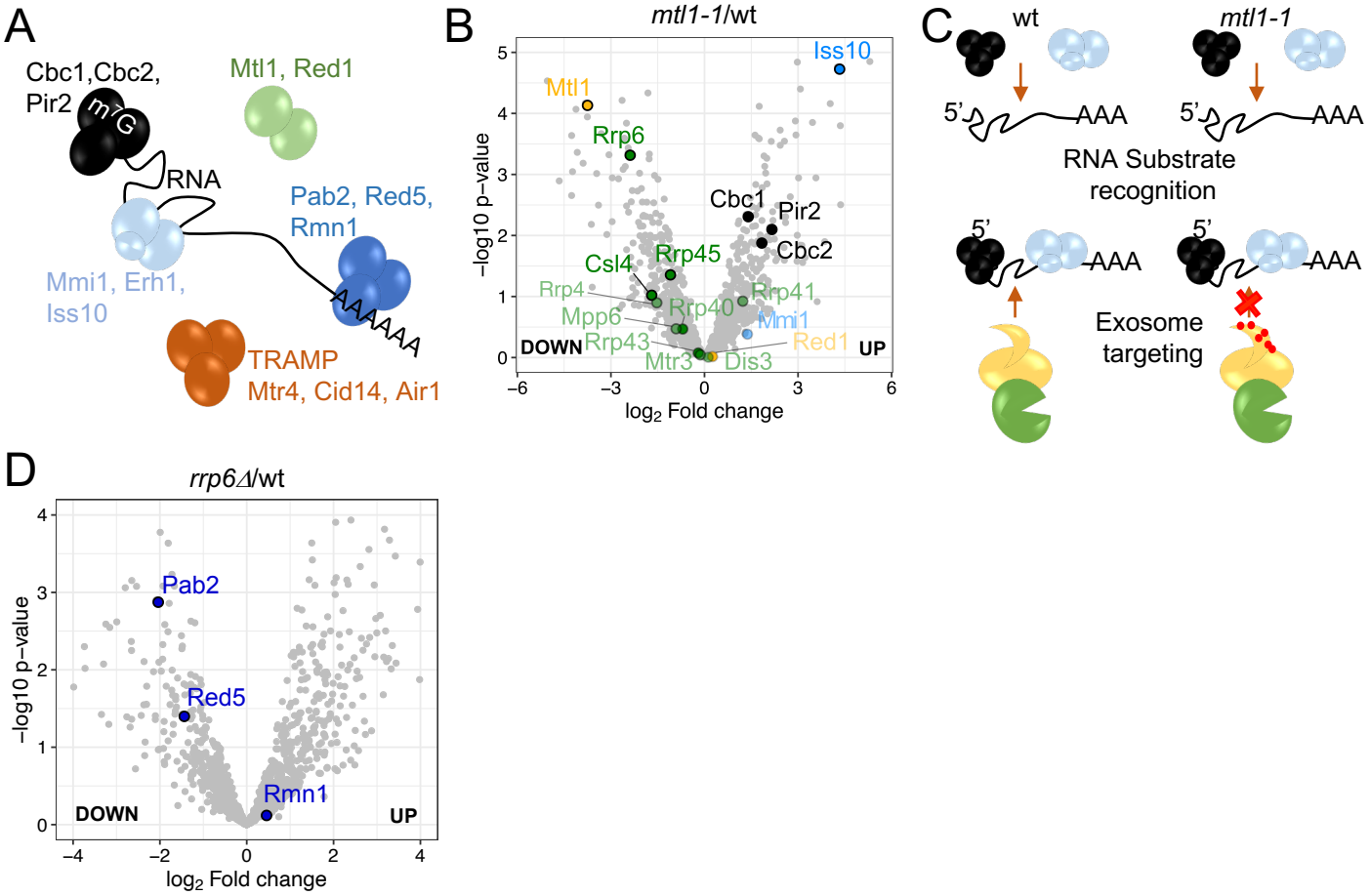
A
Cbc1,Cbc2,
Pir2
m7G
Mtl1, Red1
RNA
Pab2, Red5,
Rmn1
Mmi1, Erh1,
Iss10
AAAAAA
TRAMP
Mtr4, Cid14, Air1
B
mtl1-1/wt
Iss10
Mtl1
Rrp6
Cbc1
Pir2
Cbc2
Csl4
Rrp45
Rrp4
Rrp41
Rrp40
Mpp6
Mmi1
Rrp43
Red1
Mtr3
Dis3
DOWN
UP
−log10 p−value
log2 Fold change
C
wt
mtl1-1
5'
AAA
RNA Substrate
recognition
Exosome
targeting
D
rrp6Δ/wt
Pab2
Red5
Rmn1
DOWN
UP
−log10 p−value
log2 Fold change